AD NUMBER
AD333301
CLASSIFICATION CHANGES
TO: unclassified
FROM: confidential
LIMITATION CHANGES
TO: Approved for public release, distribution unlimited
FROM: Controlling Organization: British Embassy, 3100 Massachusetts Avenue, NW, Washington, DC 20008. Document partially illegible.
AUTHORITY
DSTL, DSIR 23/29790, 28 Jul 2008; DSTL, DSIR 23/29790, 28 Jul 2008

CONFIDENTIAL

TECHNICAL REPORT No. 79

A CORRELATION OF FORCED CONVECTION HEAT TRANSFER MEASUREMENTS ON BLUNTED CONES AND HEMISPHERES (U)

BRITISH AIRCRAFT CORPORATION

BRISTOL AIRCRAFT LIMITED
(Guided Weapons Division)

REPORT No. 79

COPY No. 48

DATE JULY 1962

TITLE

A CORRELATION OF FORCED CONVECTION HEAT TRANSFER MEASUREMENTS ON BLUNTED CONES AND HEMISPHERES FOR MACH NUMBERS UP TO 10.2 AND REYNOLDS NUMBERS UP TO 4.5×10^7

PREPARED ON BEHALF OF BRITISH AIRCRAFT CORPORATION BY:

BRISTOL AIRCRAFT LIMITED
(G.W. Aerodynamics Office)

AUTHORISATION

MR. P. D. ROSSER
(Chief Aerodynamicist, G.W.)

AUTHORS M. W. R. SEEL
R. A. BREWER
P. R. BIGNELL

BRITISH AIRCRAFT CORPORATION

BRISTOL AIRCRAFT LTD
(Guided Weapons Division)
FILTON BRISTOL

CONFIDENTIAL

THIS REPORT HAS BEEN PRODUCED UNDER
M.O.A. CONTRACT KU/20/010/C.B.31(a)

BRISTOL AIRCRAFT LIMITED

GUIDED WEAPONS ENGINEERING DEPARTMENT

TECHNICAL REPORT NO.79

A Correlation of Forced Convection Heat Transfer Measurements on Blunted Cones and Hemispheres for Mach number up to 10.2 and Reynolds numbers up to 4.5×10^7

Ref:- B78C/21/AED/1252 July 1962

SUMMARY

Data from eighteen reported Wind Tunnel and Free Flight tests on heat transfer to blunt cones and hemispheres are correlated with simple theoretical formulae. The Mach number and Reynolds number ranges for these tests are from 1.33 to 10.2 and 8×10^2 to 4.5×10^7 respectively. The blunt cone models have semi-angles between 4.75° and 15° and nose to base radius ratios between 0.125 and 0.8.

For the Free Flight tests, estimates of the error in measured heat transfer parameters are made and only points showing errors of less than 10% are retained in the analysis. The Wind Tunnel results are claimed to have errors within this limit.

In this report the Nusselt number - Reynolds number relationships are investigated and Reynolds Analogy Factors determined for a selection of the tests. In these correlations corrections for compressibility effects are made. The ratios of measured Nusselt numbers to the corresponding theoretical imcompressible Nusselt numbers are also determined. The principal conclusions made are as follows:-

1) For laminar and turbulent flow over hemispheres and hemispherical nose caps, the Nusselt and Reynolds numbers are related by simple power law formulae.

2) For laminar flow Wind Tunnel tests on conical skirts, the Nusselt numbers lie between flat plate and sharp cone theories when plotted against Reynolds number. As the value of the ratio of nose radius to base radius increases, Nusselt numbers move away from the values predicted by sharp cone theory.

3) For Free Flight tests on conical skirts with laminar flow, the Nusselt and Reynolds numbers are best correlated by sharp cone theory when they are based on the length measured from the virtual apex of the cone skirt.

4) For both Wind Tunnel and Free Flight tests on conical skirts with turbulent flow, the Nusselt and Reynolds numbers, based on the lengths measured round the model surfaces, are related by the four-fifths power law for flat plates.

5) Correlations of Free Flight measurements on conical skirts are independent of whether the local flow conditions are based on expansion from stagnation pressures corresponding to normal, or to conical shock wave conditions.

6) The ratio of experimental Nusselt numbers to theoretical incompressible Nusselt numbers, when multiplied by a factor accounting for compressibility effects, are independent of the local values of Mach number, Reynolds number and Wall temperature ratio.

7) Reynolds Analogy Factors appear to be independent of local Mach number and Reynolds number.

8) Wall temperatures, on thin skin Free Flight models, can generally be predicted to an accuracy of 10% using expressions for heat transfer coefficients given by Monaghan and Hill's wall temperature equations.

DEFENSE DOCUMENTATION CENTER
for
SCIENTIFIC AND TECHNICAL INFORMATION
(formerly Armed Services Technical Information Agency - ASTIA)

ANNOUNCING...

An Expansion of the DDC Telephone Search Service

(for official use only by organizations authorized DDC services)

On 1 January 1963 DDC (then known as ASTIA) instituted a rapid telephone search service to retrieve documents on Semiconductor Devices from its collection for engineers and scientists. The success of this service has resulted in its expansion to include the following disciplines:

Semiconductor Devices
Radiobiology
Masers
Biological Warfare
Refractory Metals

Documents which contain significant information about these subject areas have been indexed in depth, using new microthesauri of specific retrieval terms that have been developed for this rapid reference service. UNCLASSIFIED INFORMATION determined to be pertinent to a question will be given by a return telephone call. CLASSIFIED INFORMATION, bibliographies and reports, as desired, will be forwarded to the requester by the most rapid means available.

To use this search service to retrieve documents from the DDC collection that may be pertinent to your problem, call DDC (JA 5-5800, Arlington, Va.) and use the following telephone extensions which will be manned by specialists in each of the areas:

Semiconductor Devices - Ext. 2479
Radiobiology - Ext. 394
Masers - Ext. 441
Biological Warfare - Ext. 2828
Refractory Metals - Ext. 2426

DISTRIBUTION LIST

	COPY NO.
M.O.A.	
Mr. R.A. Shaw, O.B.E.	1-10
Defense Research Staff (U.S.A.)	
Mr. R.J. Monaghan Defense Research Staff, British Embassy Washington 8, D.C.	11-40
O.N.E.R.A. (Paris)	
c/o M.O.A.	41-70
A.R.C.	
Mr. R.W. Gandy	71-110
R.A.E. (Farnborough)	
Dr. L.F. Crabtree	111
Mr. J. Hamilton	112
Mr. J. Picken	113
Mr. R.L. Dommett	114
Aero Library	115
GW. Library	116
R.A.E. (Bedford)	
Library	117-118
British Aircraft Corporation	
English Electric	
Mr. A.C. Southgate (Luton)	119
Mr. R.Dickson (Warton)	120
Vickers Aircraft Limited (Weybridge)	
Mr. M.W. Salisbury	121
Royal Aeronautical Society	
Miss B.E. Beadle (Tech.Committee)	122
Bristol Aircraft Ltd.	
Mr. D.J. Farrar	123
Mr. M.J. Tayler	124
Mr. S.A.Smith	125
Mr. P.D. Rosser	126
Mr. N.F. Harpur (A.E.D. No. 7.D.O.)	127-130
G.W. T.I.B.	131
A.E.O. Library	132
Spares	133-140

CONTENTS

1. INTRODUCTION

Hypersonic flight is inevitably associated with large heat transfer rates, particularly round the forward regions of Missiles and Spacecraft. This problem has been partly solved by the introduction of blunted noses on the vehicles and by the introduction, for re-entry vehicles, of ablating heat shields. The problem of predicting the convective heat transfer distribution around blunt cones and hemispheres has therefore been extensively investigated, both theoretically and experimentally, in recent years.

Broadly, one may divide these investigations into two classes; (a) heat transfer at Mach numbers greater than ten and (b) heat transfer at Mach numbers less than ten. In the first category, real gas effects, such as dissociation, dominate the problem and the 'cool wall' approximation is valid. In the second, real gas effects are minor but the specific heats are variable. The 'cool wall' approximation is not valid in this second category of problems.

This report presents the results of an investigation into the latter class of heat transfer problems just mentioned. The investigation has been restricted to hemispheres and hemispherically blunted cones, which probably represent the most extensively tested bluff body shapes. Although no claim is made that all the experimental evidence has been investigated, it is felt that a sufficiently large number of reported tests have been analysed for the conclusions drawn to be representative.

For both Wind Tunnel and Free Flight tests the data from eighteen reported experiments on hemispheres and blunted cones has been analysed with the object of determining, for laminar and turbulent flow, the following:-

1) The variation of Nusselt number with Reynolds number and the optimum lengths on which to base these parameters.

2) The effects of local Mach number, wall temperature ratio and Reynolds number on the ratios of the compressible Nusselt numbers obtained by experiment, to the incompressible theoretical estimates.

3) For conical skirts; the effect of basing the local flow conditions on isentropic expansion from either normal or conical shock wave conditions.

4) The effect of nose to base radius ratio on the Nusselt number for conical skirts.

5) Evidence of Reynolds Analogy for a selection of the experiments analysed.

6) Comparison of theoretical and measured wall temperatures on Free Flight Models with thin skins.

Section 3 gives details of the methods used to reduce and present the data, and in Section 4 correlated results are discussed in detail. The final conclusions drawn from the investigation are presented in Section 5.

2. Notation

c	Specific heat of skin material	CHU.lb^{-1} $^{o}K^{-1}$
C_f	Local skin friction coefficient	
C_p	Specific heat of air at constant pressure	CHU.lb^{-1} $^{o}K^{-1}$
$C_{p.}$	Pressure coefficient	
G	Thermal capacity of skin $\rho_s \delta_s C_s$	CHU.ft^{-2} $^{o}K^{-1}$
h	Heat transfer coefficient based on temperature	CHU.ft^{-2} sec^{-1} $^{o}K^{-1}$
h'	Heat transfer coefficient based on enthalpy	lb. ft^{-2} sec^{-1}
i	Enthalpy	CHU. lb^{-1}
i_r	Recovery enthalpy	
k	Thermal conductivity of air	CHU.ft^{-1}sec.$^{-1}$ $^{o}K^{-1}$
M	Mach number	
Nu	Nusselt number	hs/K_1 or $h' C_{p_1} s/K_1$
Nu_s	Nusselt number based on s	$h' C_{p_1} s/K_1$
Nu_a	Nusselt number based on s_a	$h' C_{p_1} s_a/K_1$
Nu_t	Nusselt number based on s_t	$h' C_{p_1} s_t/K_1$
Nu_D	Nusselt number based on D	hD/K_1
P	Static pressure	lb.ft^{-2}
P_{oN}	Total pressure behind a normal shock wave	lb.ft^{-2}
P_r	Prandtl number	
q_a	Convective heat transfer rate	CHU.ft^{-2}.sec^{-1}
r	Recovery factor: Local body radius (Fig.1)	
R	Nose radius for blunted cone or hemisphere (Fig.1.)	ft.
R_b	Base radius of blunted cone (Fig.1.)	ft.
R_e	Reynolds number	
R_{e_s}	Reynolds number based on s	$\rho_1 U_1 s/\mu_1$
R_{e_a}	Reynolds number based on s_a	$\rho_1 U_1 s_a/\mu_1$
R_{e_t}	Reynolds number based on s_t	$\rho_1 U_1 s_t/\mu_1$
s	Surface distance measured from stagnation point (Fig.1)	ft.
s_a	Distance measured from virtual apex of blunt cone (Fig.1)	ft.
s_t	Distance measured from transition point (Fig. 1)	ft.
S	Reynolds Analogy Factor	
S_T	Stanton number	$h/\rho_1 U_1 C_p$ or $h'/\rho_1 U_1$
t	Time	sec.

T	Temperature	^{o}K (except where otherwise stated)
T_r	Recovery temperature	^{o}K
T_o	Stagnation temperature	^{o}K
U	Velocity along s co-ordinate	$(ft\text{-}sec^{1})$
β	Stagnation point velocity gradient	sec^{-1}
γ	Ratio of specific heats for air	
δ	Time interval in wall temperature calculation	sec.
ε	Surface emissivity	
θc	Cone semi-angle	degrees
μ	Dynamic viscosity	$lb.\ ft^{-1}\ sec^{-1}$
ν	Kinematic viscosity	$ft.^{2}sec.^{-1}$
ρ	Density	$lb.ft^{-3}$
σ	Deviation in a parameter: also Stefan-Boltzmann radiation constant	$CHU.ft^{-2}sec.^{-1}\ {}^{o}K^{-4}$
τ	Skin thickness	ft.
ϕ	Angular co-ordinate	degrees
ψ	Pressure gradient parameter defined in Appendix VI	

Subscripts

o	Stagnation conditions
1	Edge of boundary layer
∞	Free stream conditions
c	Compressible flow
i	Incompressible flow
f.p.	Flat plate conditions
w	Wall conditions

Superscript

*	Properties based on intermediate enthalpy conditions

N.B. All other symbols used in the report are defined in the text.

3. Data Reduction and Presentation of Results

3.1. Data Reduction Programme

Experimental data on heat transfer to blunted cones and hemispheres from eighteen sources (Refs. 1-18) has been analysed, and, since the results in these reports are presented in terms of various parameters, a data reduction programme was prepared to reduce all the data to common sets of non-dimensional parameters. Wherever possible the local flow conditions were calculated from the isentropic flow relations using experimental pressure distributions. In cases where the latter were unavailable, modified Newtonian theory was used. Referring to Fig. 1, the Newtonian pressure coefficient distribution is given by

$$C_p = C_{p_{max}} \cdot \cos^2 \phi \qquad (1)$$

$$\text{where } C_{p\ max} = \frac{P_{oN} - P_\infty}{\frac{1}{2} \cdot \gamma P_\infty M_\infty^{\ 2}} \qquad (2)$$

and P_{oN} was estimated from the normal shock wave relations with $\gamma = 1.4$.

On the conical skirts of slightly blunted cones, where the pressures were not measured, the pressure was assumed to take the conical value given by Kopal (Ref.19).

The Eckert intermediate enthalpy technique (Ref. 20) was used throughout the correlations, the relevant properties being evaluated at a temperature, T,* derived from the enthalpy, i,* which is given by

$$i^* = i_1 + 0.5\,(i_w - i_1) + 0.22\,(i_r - i_1) \qquad (3)$$

$$\text{with } i_r = i_1 \left(1 + r\,\frac{(\gamma - 1)}{2} M_1^2\right)$$

where $r = 0.85$ for laminar flow

and $r = 0.89$ for turbulent flow.

(NOTE:- For laminar flow, strictly $r = Pr^{*\frac{1}{2}}$ but $r = 0.85$ is well within the experimental accuracy and simplifies the computing)

As in the analysis carried out in Ref. 21, only experimental results having errors of 10% or less were retained in the present analysis. For the Free Flight tests, the errors in measured Stanton numbers were estimated on the same basis as that used in Refs. 21 and 22. This implies that the errors in Stanton number due to errors in the estimated pressure distributions have been ignored. The equation for estimating the errors together with detailed sources of error for Free Flight tests, given in Ref. 22, are summarised in Appendix I. Errors arising from conduction along the skin close to the stagnation point were small in cases where it was possible to assess these. A typical case is discussed in Section 4.3.1., the relevant equations being derived in Appendix II.

3.2. Presentation of Results

Details of all the tests analysed are presented in Fig. 2, which also includes a key to the symbols used in the graphs. As far as possible each source of data has been given the same symbol throughout the correlations.

It has been found convenient to present most of the results in groups as follows:-

(i) Results for hemispheres and nose caps of blunted cones with laminar flow.

(ii) As for (i) with turbulent flow.

(iii) Results for cone-skirts with laminar flow.

(iv) As for (iii) with turbulent flow.

In addition, where sufficiently large numbers of both Free Flight and Wind Tunnel results are available, these are presented separately for clarity.

3.2.1. Variation of Nusselt number with Reynolds number

The parameter $Nu^{*}Pr^{*-\frac{1}{3}}$, determined for hemispheres, hemispherical caps and cone skirts, is plotted in Figs 3-13 against Re^{*} based on various lengths. (See Fig. 1).

Figs. 3 and 4 present Wind Tunnel and Free Flight results respectively, for hemispheres and hemispherical caps with laminar flow, the abscissa in both cases being Re^{*} based on s. In Figs. 5 and 6, Wind Tunnel and Free Flight results for hemispheres and hemispherical caps with turbulent flow are plotted against Re^{*} based on s_t. (Fig. 6.)

Values of $Nu^* Pr^{*-\frac{1}{3}}$ for conical skirts with laminar flow are presented in Figs. 7-10; Figs 7 and 9 show plots of Wind Tunnel and Free Flight results respectively, against Re^* based on s, whilst Figs. 8 and 10 show these same results plotted against Re^* based on s_a . Figs 11-13, which are the final graphs in this first group, present Free Flight and Wind Tunnel results for conical skirts with turbulent flow, the abscissae being Re^* based on s, s_a and s_t respectively.

In Figs. 9 - 13, the full symbols correspond to local flow conditions based on flow through a conical shock wave originating from the vertex of a cone having the same apex angle as the cone skirt under consideration. The remaining symbols correspond to local flow conditions based on isentropic flow from stagnation conditions behind the normal section of the bow shock wave. This is essentially the method suggested by Moeckel in Ref. 23.

The equations of the theoretical curves shown in Figs. 3-13 are derived in Appendix III, and on each figure, deviations of $\pm$ 50% from the appropriate theoretical curve are shown in order to indicate the spread of the data.

3.2.2. Variation of the Laminar Heat Transfer Parameter $Nu_D/(\beta D^2/\nu)^{\frac{1}{2}}$ with s/R

Wind tunnel values of the laminar heat transfer parameter, $Nu_D/(\beta D^2/\nu)^{\frac{1}{2}}$ for hemispheres and hemispherical caps are presented in Fig. 14 as a plot against s/R, the normalised distance along the body surface. Since it depends upon the local Mach number and the local wall temperature ratio, theoretically this parameter does not collapse the results on to a single curve. However, this parameter is often used to present Wind Tunnel results of laminar heat-transfer measurements, and has been included for completeness in the present report. For the sake of comparison the theoretical curve, obtained by Korobkin in Ref. 31, is shown in Fig. 14. It should be noted here that the corresponding turbulent heat transfer parameter also fails to collapse the results on to a single curve when plotted against s/R.

3.2.3. Variation of the Ratio of Compressible to Incompressible Nusselt numbers with s/R

As stated above, the parameter $Nu_D/(\beta D^2/\nu)^{\frac{1}{2}}$ does not collapse the results when plotted against s/R. However, the

parameter $(Nu_s/Nu_i)\ (T^*/T_1)^a$ should (as shown in Appendix IV) collapse the data for hemispheres on to a straight line when plotted against s/R, with a = 0.13 for laminar flow and 0.64 for turbulent flow. By considering this particular parameter, the effects of local Mach number and wall temperature ratio should be eliminated.

In Figs. 15 and 16, Wind Tunnel and Free Flight results respectively, are presented for hemispheres and hemispherical caps with laminar flow, and in Fig. 18 results obtained from Wind Tunnel and Free Flight tests for the above bodies with turbulent flow are presented. In Figs. 15, 16 and 18 deviation of $\pm$ 50% from the theoretical line are again shown in order to indicate the spread of the data.

Wind Tunnel values for conical skirts with laminar flow are shown in Fig. 19, whilst laminar results on conical skirts obtained from Free Flight tests are shown in Figs. 20 and 21. In Fig. 20, all the local flow conditions are based on the assumption that the surface streamlines have passed through a normal shock wave, whereas in Fig. 21 it has been assumed that the surface streamlines have passed through a conical shock wave (c.f. Section 3.2.1.) Fig. 22 shows a plot of $(Nu_s/Nu_i)(T^*/T_1)^{0.64}$ against s/R for conical skirts with turbulent flow, the results being obtained from Wind Tunnel and Free Flight tests. Here, both normal and conical shock wave conditions have been used to obtain two sets of values of the above parameter; both are plotted. For cone skirts this parameter does not collapse the results on to a single line, but as explained in Appendix IV, the results should be between two lines representing the flat plate and conical limits of the parameter.

In Fig. 17, $Nu_s/Re_s^{\frac{1}{2}}$ is plotted against s/R for the results of Reference 6, with and without heat conduction effects accounted for in the region near the stagnation point. The derivation of the equation for estimating the effect of longitudinal heat conduction is presented in Appendix II.

3.2.4. Reynolds Analogy Factor

Reynolds Analogy Factor was estimated in two ways, both involving the use of experimental Stanton number measurements. (See Appendix V) The first was the evaluation of the skin friction coefficient from a flat plate formula, and the second was the correction of this coefficient for pressure gradient effects as described in Appendix VI. The function ψ, derived in Appendix VI, which describes the pressure gradient effects, is shown in Fig. 23 for a hemisphere-cone of 4.75° semi-angle with laminar flow at a free stream Mach number of 3.12 and $\frac{Tw}{To}$ ratio of 1.0.

Results for the two methods of estimating Reynolds Analogy Factor for a selected number of Wind Tunnel tests on hemispheres and hemispherical caps are presented in Figs. 24-27. Figs 24 and 26, which show plots of S against local Mach number and Reynolds number respectively, also include the boundaries within which lie the points corrected for pressure gradient effects. Values of Reynolds Analogy Factor with the correction for pressure gradient effects are presented in Figs. 25 and 27 as plots against local Mach number and Reynolds number respectively.

In Figs. 28-33, the estimates of Reynolds Analogy Factor on the conical skirts are presented, the values being obtained from the equations derived in Appendix V. These estimates are plotted against both local Mach number and local Reynolds number. Again, the full symbols of Figs. 30,31,32 and 33 correspond to local flow conditions based on flow through a conical shock wave. On all these plots the value $S = Pr^{-\frac{2}{3}}$, suggested by Colburn (Ref.24), is shown for the purpose of comparison.

3.2.5. Wall temperature measurements

Wall temperature results for four selected Free Flight tests are shown in Fig. 34. The results are presented as the ratio of measured to estimated wall temperature plotted against a reduced time of flight, $\bar{t}$, defined as

$$\bar{t} = (t - t_{min})/(t_{max} - t_{min})$$

where t_{min} = initial time for data recording

and t_{max} = time at which maximum measured wall temperature occurs.

The method used for estimating the wall temperatures is described in Appendix VII.

4. Discussion

4.1. Variation of Nusselt number with Reynolds number

4.1.1. Results for hemispheres and nose caps (Figs 3 - 6)

Both Wind Tunnel and Free Flight data for hemispheres with laminar flow correlate reasonably well with the simple hemisphere theory, as seen in Figs 3 and 4. The low points from Ref. 8, at the high Reynolds number end of Fig. 3, coming from one source, cannot be regarded as strong evidence for modifying the theory in this region. It would appear that there is some consistent error in the measurements, possibly due to conduction effects. (As shown in Appendix II, conduction may lead to an under-estimate of the Nusselt number). If these points are discarded then the theory of Ref. 25, is well verified by the experimental results in the Reynolds number range investigated.

The Free Flight tests, on the other hand, lie on the average, some 30% below the theory of Ref. 25. (Fig. 4). It may also be noted that possibly 10% of this discrepancy could be due to conduction effects, as discussed in Section 4.3.1. for the test results of Ref.6. Bearing this in mind, together with the difficulty of making Free Flight heat transfer measurements, the Free Flight data agree satisfactorily with the Wind Tunnel results.

The corresponding results for turbulent flow over hemispheres and nose caps are shown in Figs 5 and 6, for both Wind Tunnel and Free Flight tests. In Fig. 5 both the Nusselt and Reynolds numbers have been based on the distance measured from the stagnation point, s, (c.f.Fig 1) and the test data are compared with turbulent flat-plate theory. Although the simple $4/5^{ths}$ power law represents the trend of the data well, the bulk of the results are perhaps better correlated by a line about 30% below the flat plate theory.

In Ref. 26 a simple formula for turbulent flow over hemispheres is presented and the results are compared with this theory in Fig. 6. Here, in order to account for the presence of the initial run of laminar flow, both the Nusselt and Reynolds numbers have been based on the distance measured from the transion point, s_t (c.f. Fig 1) It will be observed immediately that the equation suggested in Ref. 26 is not supported by the experimental evidence

cited here. In fact, the line 30% below the flat plate theory suggested above, in connection with Fig 5, would also best correlate the results in terms of the parameters presented in Fig. 6. Since transition is impossible to predict accurately when carrying out project studies, we may recommend that, for turbulent flow over hemispheres, the best results for either Wind Tunnel or Free Flight tests will be obtained by basing the Nusselt and Reynolds numbers on s (c.f. Fig. 1) and using the simple flat-plate equation with about a 30% reduction factor.

4.1.2. Results for conical skirts (Figs. 7 - 13)

The variation of Nusselt number with Reynolds number for laminar flow over conical skirts is shown in Figs. 7 and 8, and 9 and 10, respectively for Wind Tunnel and Free Flight tests. For the Wind Tunnel results presented in Fig. 7. it will be seen that the results lie between the flat plate and sharp cone theories. This result may be anticipated intuitively, for at very large values of s/R on a blunt cone, the effect of tip blunting should be insignificant with the flow approaching fully developed conical conditions. Lees, in Ref. 27, also shows this effect as a limit to his theory for large s/R values. The existence of this trend to conical flow with increasing s/R values is discussed later in Section 4.3.2.

An alternative measure of the Nusselt and Reynolds numbers is obtained by basing them on the distance measured from the virtual apex of the cone, s_a (c.f. Fig. 1). The results based on this distance are shown in Fig. 8, and it will be observed that, for the results of Ref. 10, the correlation is almost identical with that of Fig. 7. The results of Ref. 11, however, become more evenly distributed between the flat-plate and conical theories. However, comparison of Figs 7 and 8 would indicate that there is really nothing to choose between these alternative methods of estimating the Nusselt and Reynolds numbers, at least for the Wind Tunnel test results.

The corresponding results for Free Flight tests are shown in Figs 9 and 10. Two complete sets of results are shown, the open symbols corresponding to normal shock wave conditions and the full symbols to conical shock

wave conditions (c.f. Section 3.2.1.).

Examination of the data presented in Fig. 9. indicates that the two methods suggested for determining the local flow conditions correlate the results equally well between the flap-plate and cone theories. Consequently, providing that the data is consistently analysed it would appear not to matter which assumption is made for estimating the local flow conditions. Examination of these results in conjunction with the nose to base radius ratios for each test (tabulated in Fig. 2) was also made.

This examination indicated (for the limited data of three tests) that the results are not always improved by changing from conical shock wave conditions at small R/R_b values (e.g. 0.138 for Ref. 17) to normal shock wave conditions at large values of R/R_b (e.g. 0.333 for Ref.1) So again, it may be concluded that there is little to choose between the two methods of estimating the flow conditions.

In Fig. 10 the Free Flight results are shown in terms of the Nusselt and Reynolds numbers based on the distance from the virtual apex of the cone skirts. A significant change occurs in the correlation when this is done, as can be seen by comparing Figs. 9 and 10. The results, for either set of local flow conditions, are almost uniformly distributed about the cone theory line. The low points of Ref. 17 in the Reynolds number range 10^6 to 2×10^6 may be due to conduction effects. With these few points disregarded, one may conclude that, contrary to the Wind Tunnel results, the Free Flight laminar results on conical skirts are best correlated by sharp cone theory with the Nusselt and Reynolds numbers based on s_a, the distance from the virtual apex of the cone skirt.

The Wind Tunnel and Free Flight results for turbulent flow over cone skirts are shown in Figs. 11 to 13. Both normal and conical shock wave conditions are shown. As for the laminar cases, there is little to choose between the two sets of local flow conditions, except for the results of Ref. 4. which are better when based on conical shock wave conditions. The results for the model of Ref. 17, which has a smaller R/R_b value than that of Ref. 4, are not improved by selecting conical shock wave conditions. As with the laminar results, then, we find

no consistent effect of the nose to base radius ratio on the selection of the best local flow conditions to use.

Within the scatter of the data there is little to choose between the three correlations presented in Figs. 11, 12, and 13 though the latter, with the parameters based on the distance from the transition point (s_t c.f. Fig. 1) is slightly better than the other two. It may be concluded, then, that for turbulent flow over conical skirts the results are most simply correlated in terms of the Nusselt and Reynolds number based on either of the lengths s_a or s_t . Furthermore, with the scatter in the results, no clear choice between the cone and flat plate theories can be made.

4.2. Variation of the laminar heat transfer parameter $Nu_D/(\beta D^2/\nu)^{\frac{1}{2}}$ with distance round a sphere surface (Fig. 14).

The variation of the laminar heat transfer parameter with s/R is shown in Fig. 14 for laminar flow Wind Tunnel tests on hemispheres and cone nose caps. For comparison, Korobkin's theory (Ref. 31) is also shown. It can be seen that, as predicted by this theory, the heat transfer parameter decreased with s/R. Although this parameter is independent of Reynolds number it is not independent of Mach number and wall temperature ratio effects. To compare the results with theories such as those presented in Refs. 5, 27 and 28, for example, would involve evaluating these theories for each set of conditions pertaining to the experiments under consideration. Therefore, although this parameter is frequently used to present heat transfer results obtained from laminar flow tests, it was abandoned in favour of another parameter, discussed below.

4.3. Correlations of the ratio of Compressible to Incompressible Nusselt numbers with s/R. (Figs 15 - 22).

4.3.1. Results for hemispheres and cone caps (Figs. 15 - 18)

The ratios of compressible (i.e. experimental) to incompressible Nusselt number plotted against s/R for hemispheres and nose caps are shown in Figs. 15 - 18. As shown in Appendix IV, the parameter plotted throughout these Figures (excluding Fig. 17) should be independent of all the parameters M_1, Tw/T_1, s/R and Re_s . In Fig.15 the results for laminar flow wind tunnel tests are seen to be evenly distributed about the theoretical value of unity for this parameter. Inspection of the values of

Tw/T_1, Re_s and M_1 for all the points also showed the results to be independent of these parameters although these are not noted in Fig. 15.

The corresponding Free Flight results, shown in Fig. 16, as might be anticipated from the results in Fig. 4 (discussed in Section 4.2.) lie below the theoretical value of unity. However, the data presented in terms of this parameter is again independent of s/R. The points obtained from Ref. 6, close to the stagnation point are seen to be rather low. As shown in Appendix II, if longitudinal conduction effects are ignored in estimating the Nusselt number this quantity may be under estimated. The correction for heat conduction effects was applied to the results of Ref. 6 (at a flight time of 5 secs) the result of which can be seen in Fig. 17. It can be seen that the correction to the Nusselt number can reach about 10% which could improve the low data points of Fig. 16. (It should be noted that the data for Ref. 6 shown on Fig. 16 corresponds to various flight times so that the above statement is only qualitative).

The results for turbulent flow over hemispheres and nose caps for both Wind Tunnel and Free Flight tests are shown in Fig. 18. As with the laminar flow results these are again seen to be essentially independent of s/R and examination of the conditions for each individual point on the Figure showed the results to be independent of Mach number, Reynolds number and wall temperature ratio.

4.3.2. Results for conical skirts

The Nusselt number ratios obtained from Wind Tunnel tests on conical skirts with laminar flow are shown in Fig. 19. For the results of Ref. 10 (circle points) there is a distinct trend for the results to approach the theoretical conical value as s/R becomes large. The results for Ref. 11 (triangle points), however, do not exhibit this trend. If the values of R/R_b for these two tests are compared (see Fig. 2) it will be observed that the model of Ref. 11 is effectively twice as blunt as that tested in Ref. 10. Hence, the trend towards conical flow conditions would appear to be determined primarily by the nose to base radius ratio in addition to the value of s/R.

The corresponding Free Flight results are shown for normal and conical shock wave conditions respectively in Figs. 20 and 21. Comparison of the two figures supports the earlier conclusion (made in Section 4.1.2.) that basing the local flow conditions on either conical or normal shock wave conditions makes little difference to the correlations. As found in the Nusselt number - Reynolds number plot (Fig. 9), the results fall between the cone and flat plate theories except at the lower values of s/R (≤ 11). Here the effects of nose blunting may be thought to be responsible for the spread in the data. However, the results of Ref. 1 (which correspond to $R/R_b = 0.333$) lie consistently lower than those of Ref. 4, which correspond to $R/R_b = 0.235$. Also, the points obtained from Ref. 17 ($R/R_b = 0.138$) lie slightly lower than those of Ref. 1 so that there is no consistent trend of the data in this region of s/R with nose blunting. The lower points (Refs. 17 and 1) may be low due to conduction effects previously described, or they may be due to errors in the pressure distribution (c.f. Section 3.1.)

It can also be observed that, unlike the Wind Tunnel results (c.f. Fig. 19), no trend of the Nusselt number ratio with s/R is present. Examination of the Mach number, Reynolds number and wall temperature ratios for the points presented on Figs. 20 and 21 again show the Nusselt number ratio parameter to be independent of these variables.

The corresponding Wind Tunnel and Free Flight tests for turbulent flow are shown in Fig. 22. Here again little difference is seen between the two methods of estimating the local flow conditions. Also as found for the Free Flight laminar flow results there is a large scatter in the data for values of $s/R \leq 12$. Because of the small difference between cone and flat plate theories (about 15%) for turbulent flow, the scatter in the data does not allow the detection of a trend towards the conical value of the Nusselt number ratio for large s/R values, as was possible for the laminar flow Wind Tunnel results. However, examination of the Mach number, Reynolds number and wall temperature ratios for these points show the parameter to be essentially independent of these.

4.4. Reynolds Analogy Factor Results (Figs. 23 - 33)

4.4.1. Introductory Discussion

The details of the methods used for estimating Reynolds Analogy Factor are described in Appendix V. For hemispheres the first method used was to base the local skin friction coefficients on simple formulae of the type used in the Nusselt number-Reynolds number correlations of Figs.3 &5. In the case of the hemispheres, only the laminar flow Wind Tunnel tests were examined for evidence supporting Reynolds Analogy.

The second method was to derive an expression relating the local skin friction coefficient on an axially symmetric body with either laminar or turbulent flow to that on a flat plate in terms of a pressure gradient parameter, ψ. The details of this analysis are outlined in Appendix V1. This method of evaluating the skin friction coefficients was then used as a basis for estimating Reynolds Analogy Factor as described in Appendix V. This second method, owing to the length of time involved in its calculation, was only applied to the laminar flow results as a sample test of the method.

Many authors (e.g. Lees (Ref. 27)), Vaglio-Laurin (Refs. 28, 29), and others reviewed by Phillips (Ref. 30) have derived similar pressure gradient parameters to the one derived in the present report, but their analyses are restricted to the hypersonic 'cool wall' approximation. However, the results presented here are not represented by this approximation, and thus a special analysis was carried out to determine ψ. It should be noted that the method of Steine and Wanlass (Ref. 5), though not restricted to 'cool walls' is laborious to evaluate, and was therefore unsuitable for use in the present investigation.

For estimating Reynolds Analogy Factor on cone skirts, the local skin friction coefficients were based throughout on the sharp cone equations.

4.4.2. Reynolds Analogy Factor for hemispheres and nose caps (Figs. 24 - 27)

Reynolds Analogy Factors for laminar flow over hemispheres as found using the two methods discussed in the previous section are shown in Figures 24 to 27 for the Wind Tunnel tests. Figs 24 and 25 show the results plotted against local Mach number, whereas, in Figs. 26 and 27 they are plotted against local Reynolds number. The results in Figs. 24 and 26 show immediately the great improvement in the correlation obtained by using the pressure gradient parameter ψ. However, if the results based on the use of the parameter are examined on a larger scale (Figs. 25 and 27) they are seen to lie almost wholly below the value of $Pr^{-2/3}$ suggested by Colburn in Ref. 24. For either method used to estimate Reynolds Analogy Factors on hemispheres for laminar flow, the results are seen to be virtually independent of local Mach number and Reynolds number. Although the use of the pressure gradient parameter, ψ in estimating Reynolds Analogy Factor brings the experimental results more into line with Colburn's value ($s = 1.246$), it does increase the scatter among the data points. (c.f. Figs 24 and 25, for example).

4.4.3. Reynolds Analogy Factor for conical skirts (Figs 28-33)

Figs 28 and 29 show the values of Reynolds Analogy Factor obtained from laminar flow Wind Tunnel tests on cone skirts. They are plotted, respectively against local Mach number and local Reynolds number in the two figures. The data here is so limited that no trend of Reynolds Analogy Factor with either Reynolds number or Mach number can be observed. It is worth noting, however, that the use of the pressure gradient parameter, ψ, in place of the pointed cone factor, $\sqrt{3}$, in determining Reynolds Analogy Factor for these tests might correlate the results better with the line $Pr^{-\frac{2}{3}} = 1.246$. (This is providing that the value of ψ on cone skirts does not vary significantly from that shown in Fig. 23).

The corresponding Free Flight results for laminar flow over cone skirts are shown in Figs. 30 and 31. The results based on both methods of estimating the local flow conditions are shown. Although in both Figures the data is moved to the right in going from normal to conical shock wave conditions, the value of Reynolds Analogy Factor for

each point remains virtually unaltered. The data is seen to fall below the theoretical value. This is partly due to the low values of the heat transfer data observed in Fig. 9 and also, as suggested for the Wind Tunnel tests, the results might be improved by the introduction of the pressure gradient parameter in the place of the $\sqrt{3}$ factor. Again the data shows no definite trend with either local Mach number or local Reynolds number.

To conclude the Reynolds Analogy Factor investigations, the results for turbulent flow over cone skirts are shown in Figs. 32 and 33, plotted against local Mach number and Reynolds number respectively. Again the results obtained are independent of the method of estimating the local flow conditions and also of the Reynolds and Mach numbers. This latter result was observed for the Free Flight tests on pointed cones investigated in Ref.21.

4.5. Estimation of Wall Temperatures in Free Flight for Thin Skin Models

Theoretical estimates were made of the wall temperatures attained during the flight of four rocket propelled blunt cone models and one hemisphere model. These were based on the method of Hill (Ref. 32) with the heat-transfer coefficients determined from the semi-empirical equations due to Monaghan (Ref. 33) (Details of the calculations are presented in Appendix VII.

The ratio of the measured to theoretical wall temperatures for selected measuring stations on the models of Refs. 1,2, 4 and 6 are plotted in Fig. 34 against the reduced flight time $\bar{t}$ (defined on the Figure).

Considering the simplicity of Monaghan's equations (Ref. 33) the results are very good, almost all of them lying within 10% of the perfect correlation; (i.e. the line 1.0 on Fig. 33) The method used here is thus to be recommended for estimating wall temperatures for thermally thin skins.

5. CONCLUSIONS

5.1. Nusselt number - Reynolds number Relations

i) For laminar flow over hemispheres and nose caps, for $2 \times 10^3 \leq Re_s^* \leq 3 \times 10^6$, the Wind Tunnel results correlate well with Sibulkin's formula expressed in the form

$$Nu_s^* \, Pr^{*-\frac{1}{3}} = 0.763 \; Re_s^{*\frac{1}{2}}$$

The corresponding Free Flight results follow the trend indicated by the above relation but lie 20 to 25% below the values given by this equation. The Reynolds number range for these results is $1.8 \times 10^4 \leq Re_s \leq 6.2 \times 10^6$

ii) For turbulent flow over hemispheres and nose caps, both the Wind Tunnel and Free Flight data correlate best with the flat plate equation with the constant reduced by about 30% i.e.

$$Nu_s^* \, Pr^{*-\frac{1}{3}} \simeq (0.7) \times (0.0296) \, Re_s^{*\,4/5}$$

These results, when plotted in terms of the parameters based on the distance measured from the transition point, are not correlated by van Driest's formula, namely,

$$Nu_t^* \, Pr^{*-\frac{1}{3}} = 0.042 \; Re_t^{*\,4/5}$$

iii) The results obtained from Wind Tunnel tests on cone skirts with laminar flow when correlated in terms of the parameter $Nu^* \, Pr^{*-\frac{1}{3}}$ vs Re^* lie between the flat plate and sharp cone theories. This result is independent of the lengths on which Nusselt and Reynolds numbers are based.

iv) The results obtained from Free Flight tests on cone skirts, for laminar flow, are best correlated in terms of the Nusselt and Reynolds numbers based on the distance measured from the virtual apex of the cone skirt by the equation.

$$Nu_a^* \, Pr^{*-\frac{1}{3}} = \sqrt{3} \times 0.332 \; Re_a^{*\frac{1}{2}}$$

for $10^6 \leq Re_a \leq 2 \times 10^7$

v) For both Wind Tunnel and Free Flight tests on cone skirts with turbulent flow, the scatter in the measurements is such that the data correlates equally well with either the flat plate or sharp cone theories. This is true regardless of the distance on which the Nusselt and Reynolds numbers are based.

vi) For the Free Flight tests on conical skirts, the correlations of Nusselt number with Reynolds number are independent of whether the local flow parameters are based on normal or conical shock wave stagnation conditions. This is true for both the laminar and turbulent flow results.

5.2. Results in terms of the Compressible to Incompressible Nusselt number Ratios

i) For both laminar and turbulent flow over hemispheres and nose caps, the experimental results, when reduced to the form $(Nu_s/Nu_i)\ (T^*/T_1)^a$ are independent of s/R. This is so when Nu_i is based on Sibulkin's equations for laminar flow, or with Nu_i based on the flat plate relation for turbulent flow. Furthermore, with a = 0.13 and 0.64 for laminar and turbulent flow respectively, the parameter $(Nu_s/Nu_i)\ (T^*/T_1)^a$ is essentially independent of the local values of wall temperature ratio, Mach number and Reynolds number.

ii) For cone skirts the results obtained from laminar flow Wind Tunnel tests, expressed in terms of the parameter $(Nu_s/Nu_i)\ (T^*/T_1)^{0.13}$ are independent of the local values of wall temperature ratio, Mach number and Reynolds number. Furthermore the trend of this parameter, when based on flat plate theory, towards the sharp cone value of $\sqrt{3}$ for large values of s/R appears to depend primarily on the nose to base radius ratio. Conclusive evidence of this effect could not be found because of the limited number of tests investigated.

iii) For conical skirts the results obtained from laminar flow Free Flight tests, when expressed in terms of the parameter $(Nu_s/Nu_i)\ (T^*/T_1)^{0.64}$ show no distinct trend towards the sharp cone limit at large values of s/R. Again this parameter is essentially independent of the local values of wall temperature ratio, Mach number and Reynolds number.

iv) For the turbulent Free Flight and Wind Tunnel test results on cone skirts, expressed in the form $(Nu_s/Nu_i)\ (T^*/T_1)0.64$ the scatter in the data allows no trend between the flat plate and sharp cone limits to be observed. This parameter is again found to be independent of the local values of wall temperature ratio, Mach number and Reynolds number.

v) For both laminar and turbulent flow Free Flight tests conclusions 5 (ii) to (iv) are independent of whether the data is based on normal shock wave or conical shock wave stagnation conditions.

vi) For Free Flight tests on cone skirts the parameter $(Nu_s/Nu_i)\ (T^*/T_1)^a$ has a large scatter for values of s/R less than twelve. This scatter could not be correlated with either the nose to base radius ratios nor was it completely associated with conduction effects along the model surfaces. Also some of this scatter may be due to errors in estimating the pressure distribution, as this is not always quoted precisely in Free Flight test reports.

5.3. Reynolds Analogy Factors

i) For the data investigated Reynolds Analogy Factor is virtually independent of both local Mach number and local Reynolds number.

ii) For hemispheres with laminar boundary layers, Reynolds Analogy Factor is best determined from experimental heat transfer measurements when the local skin friction coefficients are corrected for pressure gradient and body shape effects.

5.4. Wall temperatures on Thin Skin Free Flight Models

For the cases investigated, 90% of the measured wall temperatures are within 10% of the theoretical estimates for hemispherical bodies and cone skirts.

REFERENCES

1. K.C. WESTON, G.S. LUNNEY — Heat transfer measurements on an air-launched, blunted cone-cylinder rocket vehicle to Mach 9.7. NASA TM X - 84 (SEPTEMBER 1959)

2. J.J. BUGLIA — Heat transfer and boundary layer transition on a highly polished hemisphere-cone in free flight at Mach numbers up to 3.14 and Reynolds numbers up to 24 x 10^6. NASA TN D - 955 (SEPTEMBER 1961)

3. C.B. RUMSEY, D.B. LEE — Heat transfer measurements on a blunt spherical-segment nose to a Mach number of 15.1 and flight performance of the rocket-propelled model to a Mach number of 17.8 NASA TM X - 77 (NOVEMBER 1959)

4. D.B. LEE, C.B. RUMSEY, A.C. BOND — Heat transfer measured in free flight on a slightly blunted 25° cone-cylinder-flare configuration at Mach numbers up to 9.89. NACA RM L58G21 (SEPTEMBER 1958)

5. H.A. STINE, K. WANLASS — Theoretical and experimental investigation of aerodynamic heating and isothermal heat transfer parameters on a hemispherical nose with laminar boundary layer at supersonic Mach numbers. NACA TN 3344 (DECEMBER 1954)

6. J.R. HALL, K.G. SPEEGLE, R.O. PILAND — Preliminary results from a free flight investigation of boundary layer transition and heat transfer on a highly polished 8-inch-diameter hemisphere-cylinder at Mach numbers up to 3 and Reynolds numbers based on a length of 1 foot up to 17.7 x 10^6. NACA RM L57D18C (MAY 1957)

7. D.H. CRAWFORD
W.D. McCAULEY

Investigation of the laminar aerodynamic heat transfer characteristics of a hemisphere-cylinder in the Langley 11-inch hypersonic tunnel at a Mach number of 6.8.

NACA REPT. 1323
(1957)

8. M. COOPER
E. E. MAYO

Measurements of local heat transfer and pressure on six 2-inch-diameter blunt bodies at a Mach number of 4.95 and at Reynolds numbers per foot up to 81×10^6.

NASA MEMO 1-3-59L
(MARCH 1959)

9. R.D. ENGLISH
H.S. CARTER

Variation in heat transfer during transient heating of a hemisphere at a Mach number of 2.

NASA TN D-399
(JUNE 1960)

10. J.P. RHUDY
R.S. HIERS
ET AL

Investigation of hypersonic flow over blunted plates and cone.

AEDC-TN-60-93
(MAY 1960)

11. W.M. VAN CAMP

Aerodynamic heating characteristics of a nose cone at angle of attack.

McDONNELL AIRCRAFT CORPORATION,
REPT. NO. 5978
(MAY 1958)

12. K.H. GRUENEWALD
W.J. FLEMING

Laminar heat transfer to a hemisphere at Mach number 3.2 and at low heat transfer rates.

NAVORD REPORT 3980
(FEBRUARY 1956)

13. F.W. HARTWIG

Hypersonic research project. Development and application of a technique for steady state aerodynamic heat transfer measurements.

GALCIT: HYPERSONIC RESEARCH PROJECT
MEMO. NO. 37.
(JUNE 1957)

14. K.H. GRUENEWALD
R.K. LOBB
New laminar and turbulent heat transfer data applicable to practical body shapes for high Mach number flight.
PRESENTED AT U.S. NAVY SYMPOSIUM ON AEROBALLISTICS AT LAUREL, MARYLAND.
OCTOBER 1954.

15. L.T. CHAUVIN
J.P. MALONEY
Experimental convective heat transfer to a 4-inch and 6-inch hemisphere at Mach numbers from 1.62 to 3.04.
NACA RM L53 L08a
(FEBRUARY 1954)

16. I.E. BECKWITH
J.J. GALLAGHER
Heat transfer and recovery temperatures on a sphere with laminar, transitional, and turbulent boundary layers at Mach numbers of 2.00 and 4.15.
NACA TN. 4125
(DECEMBER 1957)

17. L. RABB
M.J. KRASNICAN
Effects of surface roughness and extreme cooling on boundary layer transition for 15° cone-cylinder in free flight at Mach numbers to 7.6
NACA RM E57K19
(MARCH 1958)

18. N.S. DIACONIS
R.J. WISNIEWSKI
J.R. JACK
Heat transfer and boundary layer transition on two blunt bodies at Mach number 3.12.
NACA TN 4099
(OCTOBER 1957)

19. Z. KOPAL
Tables of supersonic flow of air around cones
M.I.T. FEBRUARY 1947.

20. E.R.G. ECKERT
R.M. DRAKE, JR.
Heat and mass transfer
McGRAW-HILL BOOK COMPANY,INC.1959

21. M.W.R. SEEL
R.A. BREWER
P.R. BIGNELL
A correlation of free flight aerodynamic heat transfer measurements on pointed cones.
TECHNICAL REPORT NO. 75, BRISTOL AIRCRAFT LTD., G.W.E.D.
(JANUARY 1962)

22. R.O. PILAND
K.A. COLLIE
W.E. STONEY

Turbulent and laminar heat transfer measurements on a 1/6 scale NACA RM-10 missile in free flight to a Mach number of 4.2.

NACA RM L56C05
(JULY 1956)

23 W.E. MOECKEL

Some effects of bluntness on boundary layer transition and heat transfer at supersonic speeds.

NACA REPORT 1312
(1957)

24. A.P. COLBURN

A method of correlating forced convection heat transfer data and a comparison with fluid friction.

TRANS. AMER. INST. CHEM. ENG., VOL. 29 (1933)

25. M. SIBULKIN

Heat transfer near the forward stagnation point of a body of revolution

JNL. AERO. SCI., VOL.19 NO.8
(AUGUST 1952)

26. E.R. VAN DRIEST

On skin friction and heat transfer near the stagnation point.

AI - 2267, NORTH AMER.AVIATION INC.
(MARCH 1956)

27. L. LEES.

Laminar heat transfer over blunt nosed bodies at hypersonic flight speeds.

JET PROPULSION, VOL.26,NO.4.
(APRIL 1956)

28. R. VAGLIO-LAURIN

Laminar heat transfer on blunt nosed bodies in three dimensional hypersonic flow.

WADC-TN-58-147
(MAY 1958)

29. R. VAGLIO-LAURIN

Turbulent heat transfer on blunt nosed bodies in two dimensional and general three dimensional hypersonic flow.

WADC-TN-58-301.
(SEPTEMBER 1958)

30. R.L. PHILLIPS — A summary of several techniques used in the analysis of high enthalpy level, high cooling ratio turbulent boundary layers on blunt bodies of revolution.
THE RAMO-WOOLDRIDGE CORPORATION, GM-TM-194.
(SEPTEMBER 1957)

31. I. KOROBKIN — Laminar heat transfer characteristics of a hemisphere for the Mach number range 1.9 to 4.9
NAVORD REPORT 3841
(OCTOBER 1954)

32. P.R. HILL — A method of computing the transient temperature of thick walls from arbitrary variation of adiabatic wall temperature and heat transfer coefficient.
NACA TN 4105

33. R.J. MONAGHAN — Heat transfer by forced convection at supersonic speeds.
R.A.E. AERO TECH. NOTE NO.2259
(1953)

34. M.W.R. SEEL
R.A. BREWER — On the calculation of turbulent skin friction drag on some bodies of revolution at supersonic speeds.
BRISTOL AIRCRAFT LIMITED
GUIDED WEAPONS ENG. DEPT. TECH REPORT NO.74
(AUGUST 1961)

35. D.A. SPENCE — The growth of compresible turbulent boundary layers on isothermal and adiabatic walls.
R.A.E. AERO REPORT 2619
(JUNE 1959)

36. A.H. SHAPIRO — The dynamics and thermodynamics of compressible fluid flow VOL II
THE RONALD PRESS CO. N.Y
(1954)

37. H. SCHLICHTING — Boundary layer theory
PERGAMON PRESS LTD.
(1955)

APPENDIX I

Estimation of probable errors in measured Stanton numbers in Free Flight tests and the corresponding errors in Nusselt numbers

In Appendix 3 of Ref. 21, it is shown that in the absence of errors in local pressure measurements, the probable error in the measured local Stanton number is given by,

$$\left(\frac{\sigma ST}{ST}\right)_{total} = \left[\frac{401 + 0.16\, M_\infty^2 + (T_1(1-r)\,0.01)^2}{(T_r - T_w)^2} + \left(\frac{dt}{dT_w}\right)^2 + 0.00132\right]^{\frac{1}{2}} \text{ ++}$$

..... I (1)

(The errors assumed in individual quantities are tabulated at the end of this Appendix).

Since, in the present report, we deal exclusively with Nusselt numbers we now derive an expression relating errors in Nusselt number to those in Stanton number.

Noting that,

$$Nu = S_T . Pr . Re.$$

it is easily shown, using the relations in Appendix 3 of Ref. 21, that the probable error in the Nusselt number is given by,

$$\left(\sigma Nu/Nu\right)_{total} = \left[\left(\frac{\sigma ST}{ST}\right)^2 + \left(\frac{\sigma Pr}{Pr}\right)^2 + \left(\frac{\sigma Re}{Re}\right)^2\right]^{\frac{1}{2}}$$

..... I (2)

thus, ignoring errors in the local flow conditions implied by pressure distribution errors, we find,

$$\left(\frac{\sigma Nu}{Nu}\right)_{total} \simeq \left(\frac{\sigma ST}{ST}\right)_{total}$$

.....I (3)

so that equation I (1) also gives the probable error in the Nusselt number.

It is also necessary to show what the probable errors in Nu^* are, since this parameter is also used extensively in the correlations.

We have, $Nu = Nu^* \left(k_1 / k_1^*\right)$

.....I (4)

and, using the relations

$k \sim T^1$; $\rho \sim 1/T$ (Since p = const. across the boundary layer)

++ Temperatures in eqn. I (1) are in $^\circ R$.

equation I (4) becomes:

$$Nu^{*} = Nu \left(\rho_1 / \rho^{*}\right)^{1} \qquad \text{..... I (5)}$$

Consequently, using the previously quoted method, we find

$$\left(\frac{\sigma\, Nu^{*}}{Nu^{*}}\right) = \left[\left(\frac{\sigma\, Nu}{Nu}\right)^{2} + 1^{2}\left(\frac{\sigma\, \rho_1/\rho^{*}}{\rho_1/\rho^{*}}\right)^{2}\right]^{\frac{1}{2}} \qquad \text{..... I (6)}$$

Now, inspection of the flow data for the reports investigated here, shows that,

$$1^{2}\left[\frac{\sigma\, \rho_1/\rho^{*}}{\rho_1/\rho^{*}}\right]^{2} \ll \left[\frac{\sigma\, Nu}{Nu}\right]^{2} \qquad \text{..... I (7)}$$

Consequently,

$$\left(\frac{\sigma\, Nu^{*}}{Nu^{*}}\right) \simeq \left(\frac{\sigma\, Nu}{Nu}\right) \qquad \text{..... I (8)}$$

Finally, the errors in Re^{*} and Pr^{*} due to errors in measured wall temperature can be shown to have no significant effect on the correlations.

Table of probable errors (After Ref. 22).

Quantity	Error
T_w	20°R
T shield	20°R
ρ_∞	0.013 ρ_∞
T_∞	1°R
U_∞	4 ft/sec
dT_w/dT	1° R/sec
τ	0.03 τ
ρ_1/ρ_∞, T_1/T_∞, U_1/U_∞	0
ϵ_s	0.02

Note: $1^{\circ}R \simeq 0.5^{\circ}K$

Appendix II

Estimation of the effect of longitudinal conduction on Nusselt number.

In the absence of circumferential heat flow and radiation the heat balance equation for a typical surface element may be written

$$q_a = (\rho\ c\ \tau)_s \frac{\partial T_w}{\partial t} - k_s \tau \left\{ \frac{1}{y} \cdot \frac{dy}{ds} \cdot \frac{\partial T_w}{\partial s} + \frac{\partial^2 T_w}{\partial s^2} \right\} \quad \ldots\ldots\ \text{II (1)}$$

where q_a = convective heat transfer rate per unit area per unit time.

y = body perimeter in planes normal to the axis.

Defining a local Nusselt number by,

$$Nu_1 = q_a\ s/k_1\ (T_r - T_w) \quad \ldots\ldots\ \text{II (2)}$$

equation II (1) may be written as

$$Nu_1 = (Nu)_{exp} - \frac{k_s\ \tau\ s}{k_1\ (T_r - T_w)} \Omega \quad \ldots\ldots\ \text{II (3)}$$

where Ω is the term in curly brackets in equation II (1) and $(Nu)_{exp}$ is the experimentally determined Nusselt number neglecting conduction and radiation effects, i.e.,

$$(Nu)_{exp} = (\rho c \tau)_s \cdot \frac{s}{k_1\ (T_r - T_w)} \quad \ldots\ldots\ \text{II (4)}$$

If the Nusselt number is based on enthalpy in place of temperature, equation II (3) becomes

$$Nu_1 = (Nu)_{exp} - \frac{k_s\ \tau\ s\ \bar{C}_p\ \Omega}{k_1\ (i_r - i_w)} \quad \ldots\ldots\ \text{II (5)}$$

and $\bar{C}_p$ is such that

$$\bar{C}_p\ (T_r - T_w) = (i_r - i_w) \quad \ldots\ldots\ \text{II (6)}$$

Consequently, depending upon the sign of Ω in equation II (5) the experimentally determined Nusselt number can either over - or underestimate the true Nusselt number, if conduction is ignored.

Appendix III

Summary of the equations used in the Nusselt number - Reynolds number correlations.

1. Hemispheres and nose caps.

For laminar flow over hemispheres an equation relating the local Stanton and Reynolds number is given in Ref. 25 in the form,

$$S_T = 0.763\, P_r^{-0.6}\, Re_s^{\frac{1}{2}} \qquad \text{III (1)}$$

Replacing $P_r^{-0.6}$ by $P_r^{-2/3}$ ++ and introducing intermediate enthalpy conditions to account for compressibility effects, this equation becomes

$$S_T^*\, P_r^{*2/3} = 0.763\, Re_s^{*-\frac{1}{2}}$$

Noting that the Stanton and Nusselt numbers are related by

$$N_{u_s}^* = S_T^*\, P_r^*\, Re_s^* \qquad \text{III (2)}$$

the Nusselt number for hemispheres in compressible flow is found to be

$$N_{u_s}^*\, P_r^{*-1/3} = 0.763\, Re_s^{*\frac{1}{2}} \qquad \text{III (3)}$$

For turbulent flow over hemispheres, the equation given in Ref.26, in terms of local flow conditions is

$$S_T = 0.042\, P_r^{-2/3}\, Re_s^{-1/5} \qquad \text{III (4)}$$

Following the same procedure as for laminar flow, the Nusselt number based on intermediate enthalpy conditions for turbulent flow over hemispheres is found from III (4) to be

$$N_{u_s}^*\, Pr^{*-1/3} = 0.042.\, Re_s^{*4/5} \qquad \text{III (5)}$$

To correct for the initial run of laminar flow the Nusselt and Reynolds numbers are based on the distance s_t measured from the transition point (Fig. 1) so that equation III (5) becomes

$$N_{u_t}^*\, P_r^{*-1/3} = 0.042\, R_{e_t}^{*4/5} \qquad \text{III (6)}$$

++ This has been done merely to preserve the parameter $P_r^{*-1/3}$ throughout the correlations.

2. Flat Plate

For laminar flow the Nusselt and Reynolds numbers, based on intermediate enthalpy conditions are related by

$$N_{u_s}^{*} \; P_r^{*\,-1/3} = 0.332 \; R_e^{*\,\frac{1}{2}} \qquad \text{III (7)}$$

and for turbulent flow they are related by

$$N_u^{*} \; P_r^{*\,-1/3} = 0.0296 \; R_e^{*\,4/5} \qquad \text{III (8)}$$

with Nu and Re based on either s or s_t respectively.

3. Cone Skirts

For cone skirts the flat plate equations are used, replacing the constants by

$\sqrt{3} \times 0.332$ for laminar flow

and 1.15×0.0296 for turbulent flow.

In addition to basing the Nusselt and Reynolds numbers on the distances s and s_t (for turbulent flow), they may also be based on the distance measured from the virtual apex of the cone skirts, s_a. (See Fig. 1.)

Appendix IV

Relations between the compressible and incompressible Nusselt numbers for laminar and turbulent flow.

For a flat-plate, in either laminar or turbulent flow the local Nusselt number and local Reynolds number are related in incompressible flow by an equation of the form,

$$Nu_i \sim Pr_1^{1/3} (Re_1)^n \qquad \text{IV (1)}$$

with $n = 4/5$ for turbulent flow and $\frac{1}{2}$ for laminar flow.

Following the reference temperature correction technique due to Eckert (Ref. 20), we first find an 'intermediate' Nusselt number, given by a relation of the form,

$$Nu^* \sim Pr^{*1/3} (Re^*)^n \qquad \text{IV (2)}$$

Where the flow properties are evaluated at a temperature T^* corresponding to the enthalpy i^* given by

$$i^* = i_1 + 0.5 (i_w - i_1) + 0.22 (i_r - i_1) \qquad \text{IV (3)}$$

The Nusselt number in compressible flow is related to Nu^* by,

$$(Nu)_c = Nu^* (k^*/k_1) \qquad \text{IV (4)}$$

Hence, combining equations IV (1), (2) and (4), the ratio of compressible to incompressible Nusselt numbers is found as,

$$Nu_c/Nu_i = (Pr^*/Pr_1)^{1/3} (Re^*/Re_1)^n (k^*/k_1) \qquad \text{IV (5)}$$

finally, making use of the following simplifications,

$$Pr^* \simeq Pr_1 \; ; \; \mu \sim T^{0.7} \; ; \; k \sim T^{0.723}$$

then equation IV (5) becomes,

$$Nu_c/Nu_i = (T^*/T_1)^{-a} \qquad \text{IV (6)}$$

where $a = 0.13$ for laminar flow
$a = 0.64$ for turbulent flow.

Now, if for hemispheres in laminar flow, the experimental values of Nu_s^* correlated perfectly with the equation:-

$$Nu_s^* = 0.763 Pr^{*\,1/3} Re_s^{*\,\frac{1}{2}} \qquad \text{IV (7)}$$

then, providing Nu_i is determined from the incompressible form of the above equation, the experimental results plotted in the form $(Nu_s/Nu_i)\ (T^*/T_1)^{0.13}$ vs. s/R should lie about the line 1.0.

Similarly, if for hemispheres in turbulent flow, the flat plate equation best correlates the results in terms of $Nu_s^*\ P_r^{*\,-1/3}$ vs. Re_s^*; then the parameter $(Nu_s/Nu_i)\ (T^*/T_1)^{0.64}$ should collapse the experimental data about the line unity, when plotted against s/R. This is providing, of course, that Nu_i is based on the flat plate equation:-

$$Nu_i = 0.0296\ P_r^{*\,1/3} \cdot Re_s^{4/5} \qquad \text{IV (8)}$$

For conical skirts one may expect, for large values of s/R and slight degrees of nose-blunting (i.e. $R/R_b << 1$), that the heat transfer conditions will approach those for a pointed cone. In the correlations of the parameter $(Nu_s/Nu_i)\ (T^*/T_1)^a$ vs. s/R for cone skirts, the values of Nu_i were determined from flat plate equations. Consequently, in regions where the flow approaches pointed cone conditions the parameter $(Nu_s/Nu_i)\ (T^*/T_1)^a$ would take a value different from unity. Intuitively this parameter, for, cone skirts, should be in the ranges

$$1.0 \leqslant (Nu_s/Nu_i)\ (T^*/T_1)^{0.13} \leqslant \sqrt{3} \quad \text{for laminar flow}$$

and $1.0 \leqslant (Nu_s/Nu_i)\ (T^*/T_1)^{0.64} \leqslant 1.15$ for turbulent flow.

Finally we note that, by using the intermediate enthalpy correction technique, the function $(T^*/T_1)^a$ should account for both Mach number and wall temperature effects.

APPENDIX V

Derivation of Reynolds Analogy Factor from measured values of Stanton number

1) Laminar Flow

Reynolds Analogy Factor, S, is related to the Stanton number and skin friction coefficient by the equation

$$S = S_T / (C_f/2) \qquad \text{V (1)}$$

Noting that C_f, for compressible flow, can be expressed in the form:-

$$C_f/2 = (\rho^*/\rho_1)\, c\, (R_{e_s}{}^*)^{-\frac{1}{2}} \qquad \text{V (2)}$$

Reynolds Analogy Factor becomes

$$S = S_T / \left\{ (\rho^*/\rho_1)\, c\, (R_{e_s}{}^*)^{-\frac{1}{2}} \right\} \qquad \text{V (3)}$$

where S_T is the experimentally determined Stanton number and c takes the values tabulated at the end of this Appendix.

2) Turbulent Flow

Assuming the Prandtl-Schlichting formula for the compressible skin friction coefficient in turbulent flow, (Ref 37), equation V (1) gives Reynolds Analogy Factor in the form

$$S = S_T / \left\{ (\rho^*/\rho_1)\, c\, (\log_{10} R_{e_s}{}^*)^{-2.45} \right\} \qquad \text{V (4)}$$

where c takes the values tabulated below.

3) Values of the constant, c

	FLAT PLATE	SHARP CONE	HEMISPHERE
Laminar Flow	0.332	$\sqrt{3} \times 0.332$	$(0.332)/\psi$
Turbulent Flow	0.144	1.15×0.144	$(0.144)/\psi$

where ψ is the pressure gradient parameter derived in Appendix VI

For hemispheres with laminar flow both the 'flat-plate' and 'hemisphere' values of c were used in the Reynolds Analogy Factor calculations.

For hemispheres with turbulent flow the 'flat-plate' values of c were used and for the cone skirts, in all cases the 'sharp cone' values of c were used for determining Reynolds Analogy Factor.

Appendix VI

The Effect of Pressure Gradients on Skin Friction Coefficients for Laminar and Turbulent Flow on Blunted Cones.

1. The skin friction coefficient for turbulent flow.

It is shown in Ref. 34, that by using a modified form of the Stewartson - Illingworth transformation introduced by Spence in Ref. 35, the momentum equation for axially symmetric turbulent flow may be expressed in the form:-

$$\frac{d\bar{\Theta}}{ds} + \bar{\Theta}\left\{\frac{B}{U_1}\frac{d\bar{U}}{ds} + \frac{1}{r}\frac{dr}{ds}\right\} = c\,(1+m)\,(\zeta)^{\alpha}.\,(\xi)^{-\beta} \qquad \text{VI (1)}$$

where

$\bar{\Theta} = \bar{\theta}\,(\bar{U}_1\bar{\rho}/\gamma_o)^m$

$\bar{\theta} = \theta\,(\zeta)^k$

$\bar{U}_1 = U_1\,(\zeta)^{-1/2}$

θ = momentum thickness

$B = (T_w/T_1)\,H_i + (T_r/T_1) - 1$

H_i = shape parameter for incompressible flow

$\zeta = T_1/T_o$

$\xi = T^*/T_o$

c, m, α, β = constants

(The other symbols are as defined for the main report).

For the isothermal wall case, in which we are interested, Spence showed that k and 1 take the values

$$k = 1 - r/2 + 1/(\gamma - 1)$$
$$1 = 1 \qquad \text{VI (2)}$$

Equation VI (1) may be integrated to give

$$\bar{\Theta} = \frac{c(1+m)}{f(s)}\int_o^s f(s).\,ds \qquad \text{VI (3)}$$

where $f(s) = (M_1)^B.\,(\zeta)^{\delta}\,(\xi)^{-\beta}\,(r)^{m+1}$

and $\delta = \alpha + (1 - 1)\,B/2$

Now, it is also shown in Ref. 35 that the local skin friction coefficient may be found from the relation

$$\frac{C_f}{2} = \frac{C.\theta}{\Theta} \qquad \text{VI (4)}$$

where $\Theta = (\zeta)^{-\alpha}(\xi)^{\beta}\ \bar{\theta}$ VI (5)

Finally, combining equations VI (3), (4) and (5), the local skin friction coefficient is found to be

$$\frac{C_f}{2} = \left\{ Z(s) \right\} \left[\frac{\int_0^s \delta f(s)\ ds}{f(s)} \right]^{-m/(m+1)} \qquad \text{VI (6)}$$

where

$$Z(s) = (\xi)^{-1/m+1} \left(\frac{\mu^*}{\rho_1 U_1} \right)^{m/m+1} \left(\frac{c\ (1+m)}{(1+m)} \right)^{1/m+1} \qquad \text{VI (7)}$$

2. The skin friction coefficient for laminar flow.

A completely analogous method to that outlined above for finding the turbulent skin friction coefficient may be applied to the laminar flow case. In order to do this it is only necessary to adjust the values of the constants α, β, B, m and c and to make a simple postulation discussed below. It should be noted that B, α and β depend upon the value of m (see Ref.35) and that c and m are the constants in the equation relating the friction coefficient on a flat-plate to the momentum thickness Reynolds number, i.e.

$$\frac{C_f}{2} = c\ (Re_\theta)^{-m} \qquad \text{VI (8)}$$

For the turbulent flow analysis, Spence showed, by assuming a quadratic temperature - velocity relationship, which is not restricted to unit Prandtl number, that the compressible and incompressible shape parameters are related by

$$H = (T_w/T_1)\ H_i + (T_r/T_1) - 1 \qquad \text{VI (9)}$$

Now, for laminar flow with unit Prandtl number, it can be shown (e.g. Ref. 36) that the temperature - velocity relationship across the boundary layer is a quadratic of the form

$$T = T_w + (T_o - T_w)\left(\frac{U}{U_1}\right) - (T_o - T_1)\left(\frac{U}{U_1}\right)^2 \qquad \text{VI (10)}$$

This becomes identical with the relation assumed for turbulent boundary layers which leads to equation VI (9) if T_o is replaced by T_r.

Thus, if we make this modification to equation VI (10) without attempting a rigorous justification, the analysis for the laminar boundary layer is formally identical with that outlined for the turbulent boundary layer. Hence, equation VI (6) gives the skin friction coefficient for either laminar or turbulent flow depending upon the values selected for the constants.

3. Derivation of the pressure gradient parameter, ψ , relating skin friction coefficients on an axially symmetric body to those on a flat plate.

The function z (s) defined in equation VII (7) may be written in the form

$$z(s) = A\,(\rho^*/\rho_1)\,(\rho^* U_1 s/\mu^*)^{-m/m+1}\,(s)^{m/m+1} \qquad \text{VI (11)}$$

where $$A = \left\{ c\,(1+m) \right\}^{1/m+1} \Big/ \; (m+1) \qquad \text{VI (12)}$$

We note that with $m = \frac{1}{4}$ and $c = 0.0128$ (turbulent flow) A takes the value 0.0296 and that with $m = \frac{1}{2}$ and $c = 0.2205$ (laminar flow) A takes the value 0.332. Thus z (s) may be written in terms of the compressible skin friction coefficient for a flat plate as follows,

$$z(s) = \left(\frac{c_f}{2} \right)_{f.p.} \left(\frac{1}{s} \right)^{-m/m+1} \qquad \text{VI (13)}$$

If the value of z (s) found in equation V1 (13) is substituted into equation VI (6), the relationship between the skin friction coefficients on an axially symmetric body and a flat plate is found to be,

$$\frac{C_f}{2} = \left(\frac{C_f}{2}\right)_{f.p.} \left\{ \frac{1}{s.\ f\ (s)} \int_o^s f(s).\ ds \right\}^{-m/m+1} \quad \text{VI (14)}$$

The term in curly brackets in the above equation can now be identified as a combined pressure gradient and body shape parameter. For brevity this is given the symbol Ψ and is referred to simply as the pressure gradient parameter. Consequently we have:-

$$\psi = \left\{ \frac{1}{s\ \ f\ (s)} \int_o^s f\ (s).\ ds \right\}^{-m/m+1} \quad \text{VI (15)}$$

The values of the constants α , β , m, and B are as follows:-

	Laminar Flow	Turbulent Flow
α	3.85	3.269
β	0.3	0.825
m	1	0.25
B	$5.18 \frac{Tw}{To} + 3$	1.875 Tw/To+2.25

A computer programme was written to evaluate ψ for hemispheres and hemispherically blunted cones. In all cases the modified Newtonian pressure distribution was assumed in the computation of ψ . Also, it was necessary to take a mean value of Tw/To in the calculations since the theory assumes isothermal wall conditions.

APPENDIX VII

Estimation of Wall Temperatures

Providing that the skin can be regarded as thermally thin, Hill showed in Ref. (32) that the wall temperature at the instant t_m is related to that at the previous instant t_{m-1}, by the equation

$$\left(T_w\right)_m = \frac{h_m T_{rm} + \left(hT_r - hT_w + 2GT_w / \delta\right)_{m-1} - rm - r_{m-1}}{(2/\delta)\, G_m + h_m} \quad \text{VII (1)}$$

where $G = \rho_s C_s \tau$

and r = radiation rate $= \varepsilon \sigma T_w^4$

The variation of specific heat, c, with temperature was included in the calculations.

The heat-transfer coefficients for laminar and turbulent flow were determined, respectively, from the following semi-empirical relations (Ref. 33),

$$h = 0.0368\, (Re_s)^{-1/5}\, (T_1 / T_w)^{0.46}\, (\rho_1 \mu_1 C_p)_1$$

(turbulent flow) VII (2)

$$h = 0.413\, (Re_s)^{-\frac{1}{2}}\, (T_1 / T_w)^{0.15}\, (\rho_1 \mu_1 C_p)_1$$

(laminar flow) VI (3)

where a Prandtl number of 0.7 has been assumed.

A computer programme was written to solve the above set of equations with the iterations repeated until

$$\left\{ \left(T_w\right)_m - \left(T_w\right)_{m-1} \right\} < \pm 0.1^{\circ}K$$

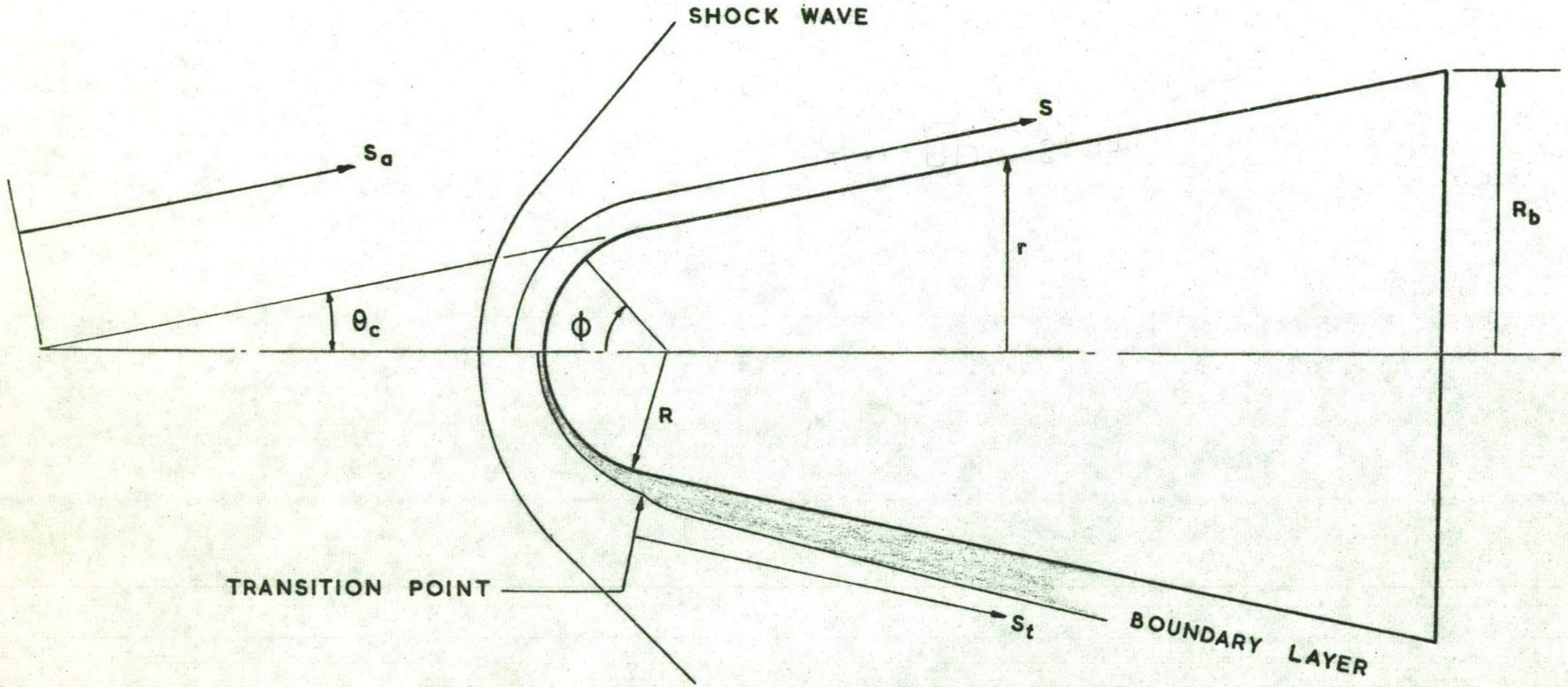

FIG. 1 GEOMETRY OF THE HEMISPHERE – CONE.

FIG. 2

REF	SYMBOL	MODEL	TEST	θ_c	R/R_b	M_∞	$Re_s \times 10^{-6}$
1	⊙	H – C	F. F.	7·5	0·333	4·5 – 6·85	0·747 – 3·02
2	△	H – C	F. F.	14·5	0·740	2·32 – 3·14	0·307 – 10·9
3	▽	H	F. F.	–	1·0	3·95 – 10·2	0·011 – 0·057
4	⊡	H – C	F. F.	12·5	0·235	2·97 – 3·28	1·15 – 4·06
5	◇	H	W. T.	–	1·0	1·97	0·15 – 1·31
6	+	H	F. F.	–	1·0	2·15 – 2·96	0·110 – 4·36
7	×	H	W. T.	–	1·0	6·8	0·0008 – 0·120
8	D	H	W. T.	–	1·0	4·95	0·293 – 2·32
9	d	H	W. T.	–	1·0	2·01	0·057 – 4·54
10	⊙	H – C	W. T.	15	0·1254	8·08	0·011 – 0·069
11	△	H – C	W. T.	10	0·250	2·47 – 4·53	0·162 – 2·97
12	⌓	H	W. T.	–	1·0	3·21	0·015 – 0·126
13	▽	H	W. T.	–	1·0	7·8	0·018 – 0·027
14	⊡	H	W. T.	–	1·0	1·9 – 4·87	0·006 – 0·390
15	◇	H	W. T.	–	1·0	1·62 – 3·04	0·016 – 4·08
16	⊙	H	W. T.	–	1·0	2·0 – 4·15	0·079 – 2·33
17	d	H – C	F. F.	7·5	0·138	1·33 – 7·08	1·52 – 44·6
18	⊣	H – C	W. T.	4·75	0·80	3·12	0·012 – 0·184

NOTATION H – C HEMISPHERE – CONE F.F FREE FLIGHT TEST

H HEMISPHERE W.T. WIND TUNNEL TEST

FIG. 2 TABLE SUMMARISING TEST DATA AND MODEL GEOMETRY INCLUDING SYMBOLS USED IN THE CORRELATIONS.

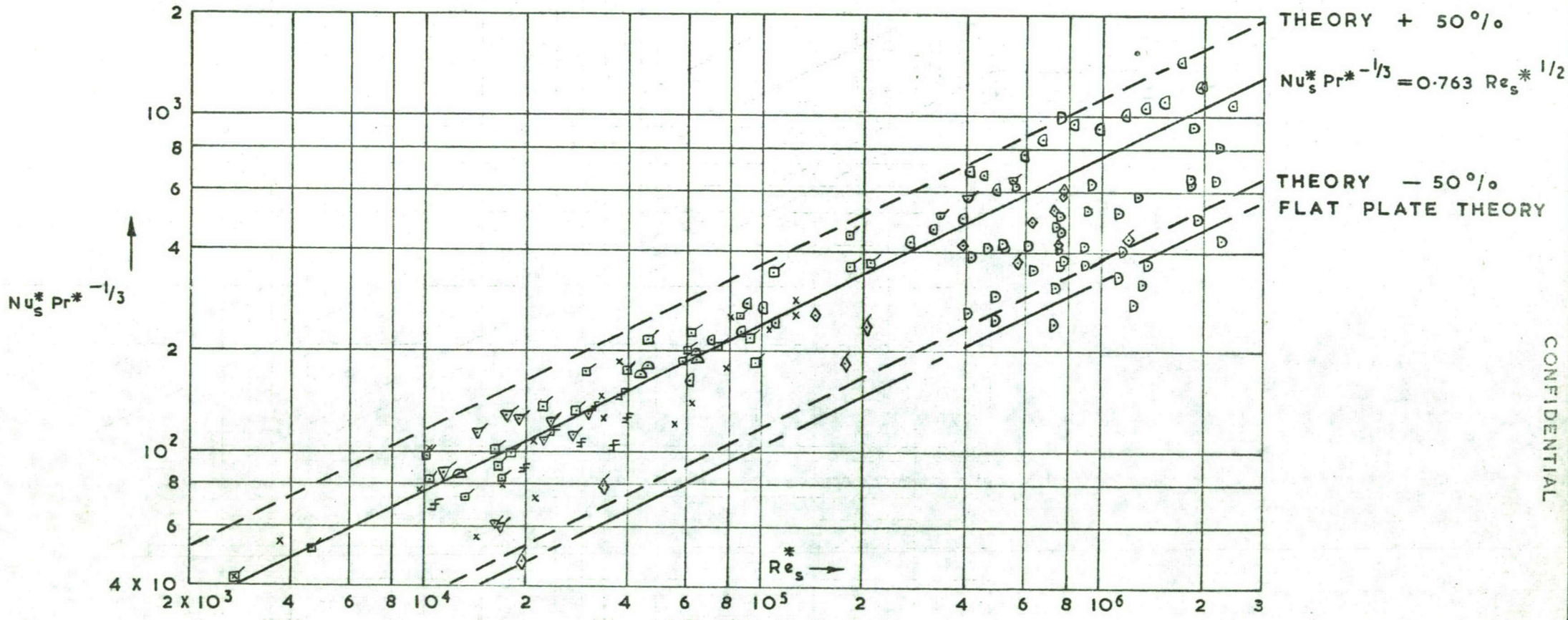

FIG. 3. VARIATION OF $Nu_s^* Pr^{*-1/3}$ WITH Re_s^* FOR WIND TUNNEL TESTS ON HEMISPHERES AND BLUNT CONE NOSE CAPS. LAMINAR FLOW.

CONFIDENTIAL

FIG. 3.

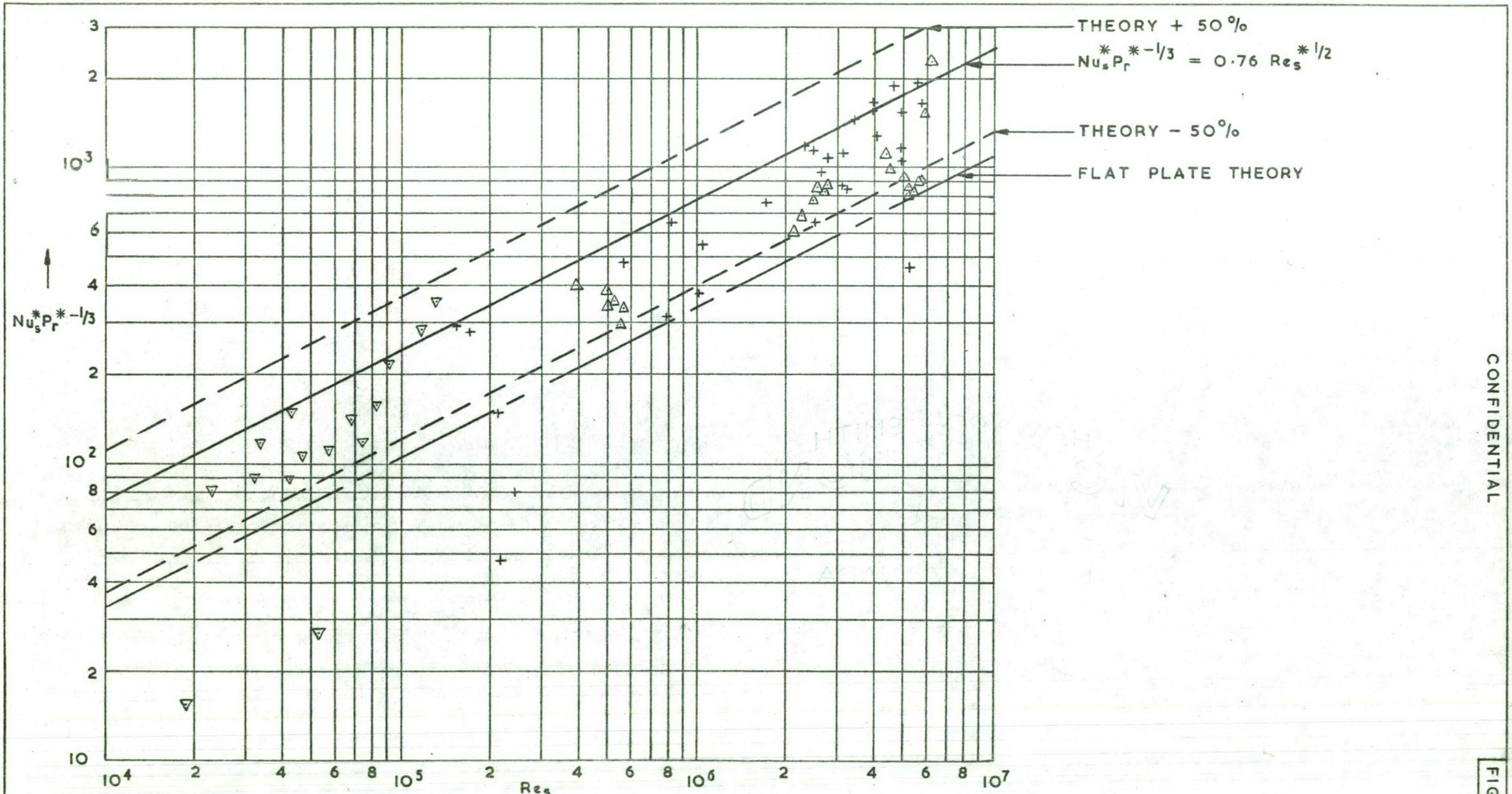

FIG. 4. VARIATION OF $Nu_s^* P_r^{*-1/3}$ WITH Re_s^* FOR FREE FLIGHT TESTS ON HEMISPHERES AND BLUNT CONE NOSE CAPS. LAMINAR FLOW.

CONFIDENTIAL

FIG. 4.

FREE FLIGHT TESTS:- Δ, +

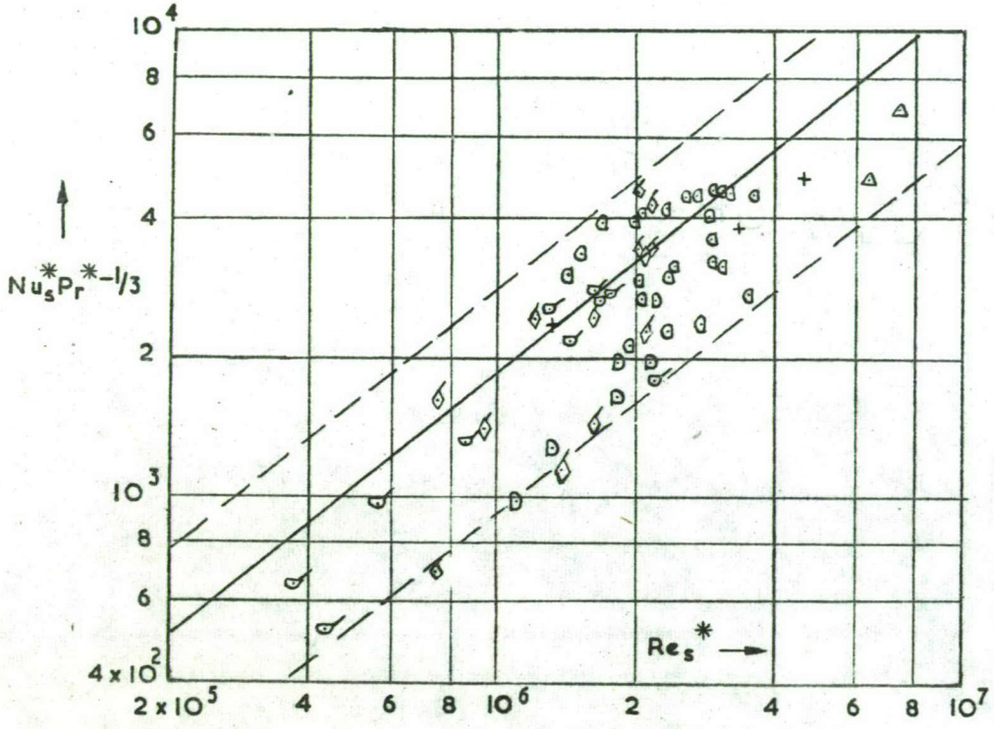

——— $Nu_s^* Pr^{*-1/3} = 0.0296\ Re_s^{*4/5}$

– – – – – THEORY (+) OR (–) 50%

FIG. 5

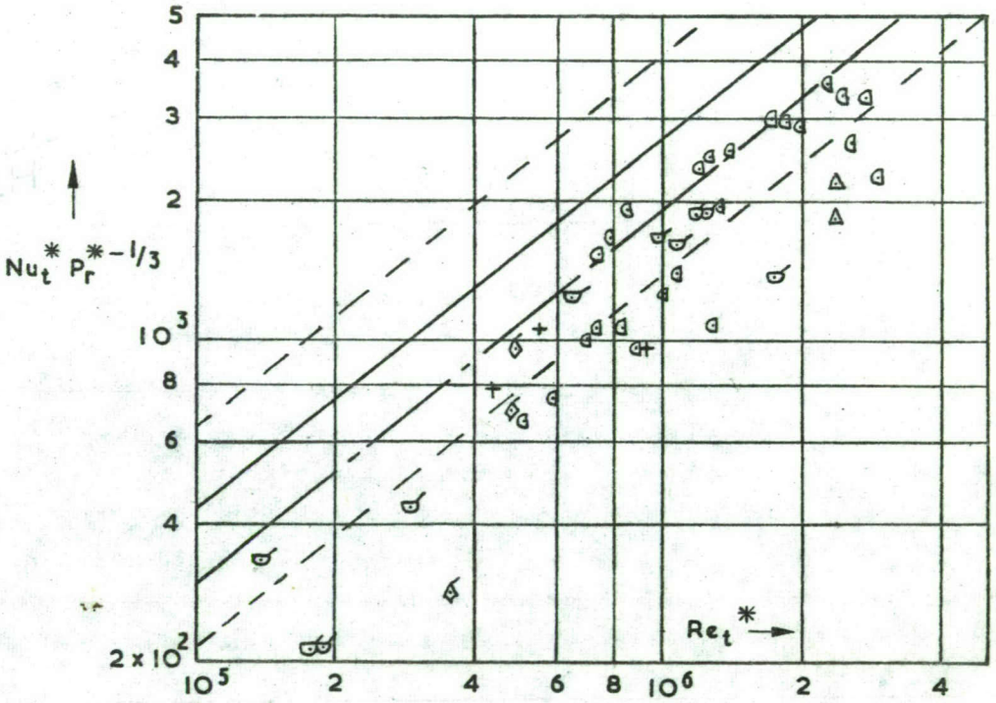

——— $Nu_t^* Pr^{*-1/3} = 0.042\ Re_t^{*4/5}$

– – – – – THEORY (+) OR (–) 50%

—·— FLAT PLATE THEORY

FIG. 6

FIGS. 5 & 6. VARIATION OF $Nu_s^* Pr^{*-1/3}$ & $Nu_t^* Pr^{*-1/3}$ WITH Re_s^* AND Re_t^*, RESPECTIVELY, FOR WIND TUNNEL AND FREE FLIGHT TESTS ON HEMISPHERES AND BLUNT CONE NOSE CAPS. TURBULENT FLOW.

CONFIDENTIAL

FIGS. 5 & 6.

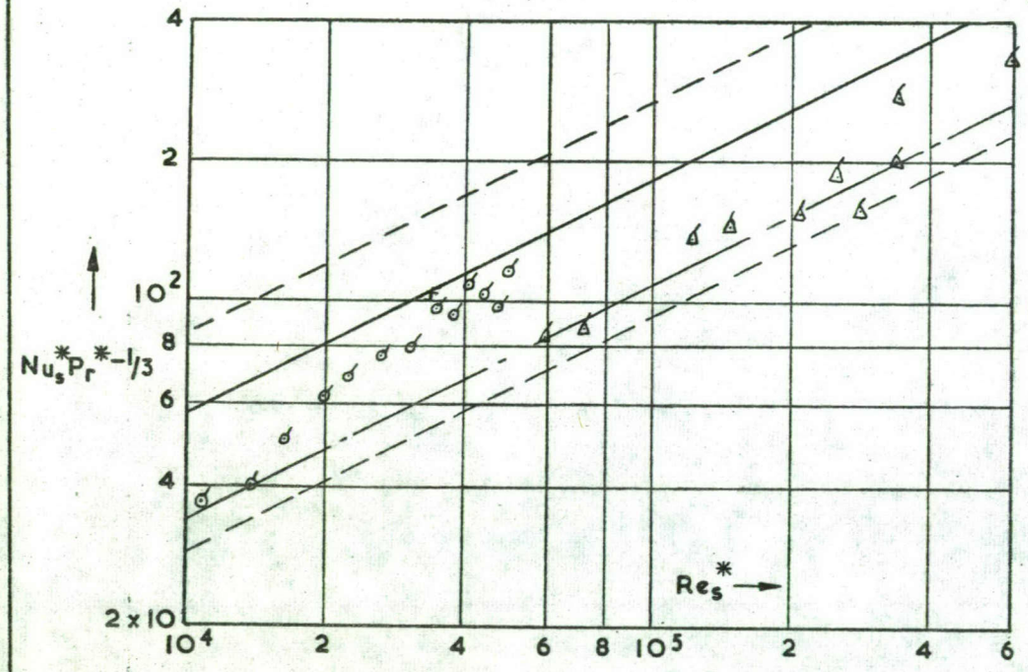

FIG. 7.

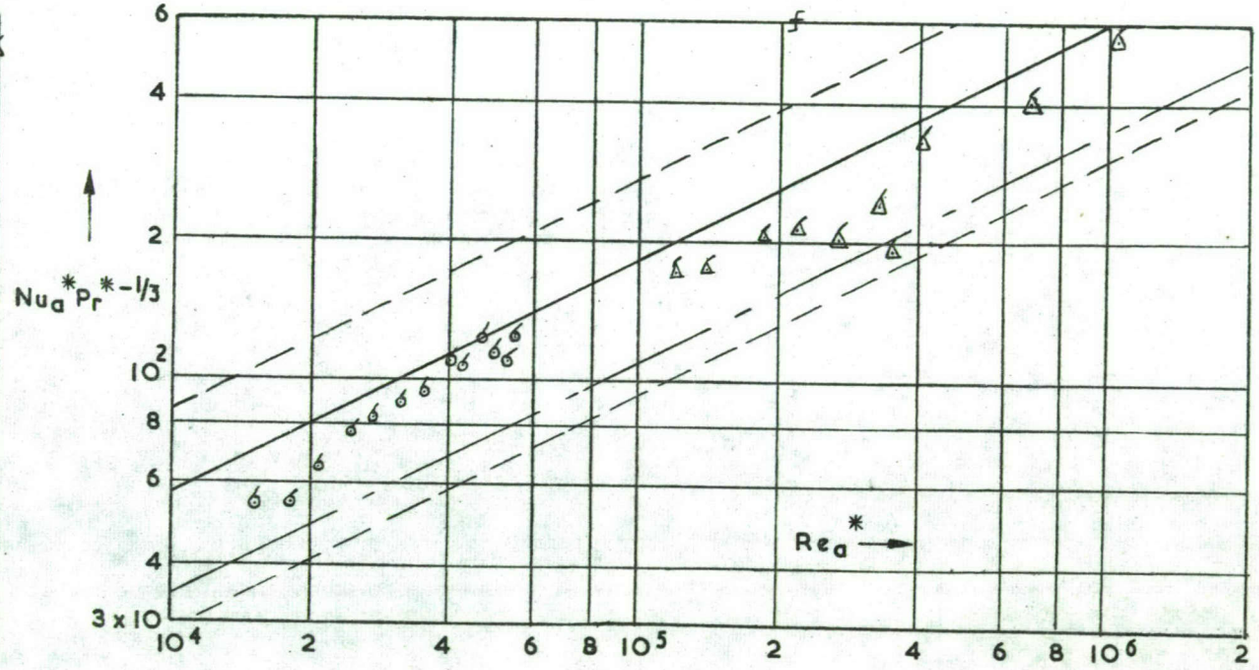

FIG. 8.

——— CONE THEORY, $\sqrt{3}$ x FLAT PLATE THEORY

—·— FLAT PLATE THEORY, $Nu^* Pr^{*-1/3} = 0{\cdot}332\ Re^{*1/2}$

- - - - - CONE THEORY + OR − 50%

FIGS. 7 & 8. VARIATION OF $Nu_s^* Pr^{*-1/3}$ AND $Nu_a^* Pr^{*-1/3}$ WITH Re_s^* AND Re_a^* RESPECTIVELY, FOR WIND TUNNEL TESTS ON CONE SKIRTS. LAMINAR FLOW.

FIGS. 7 & 8

NORMAL SHOCK WAVE CONDITIONS:- ◁ □ ○ △ CONICAL SHOCK WAVE CONDITIONS:- ◁ ■ ●

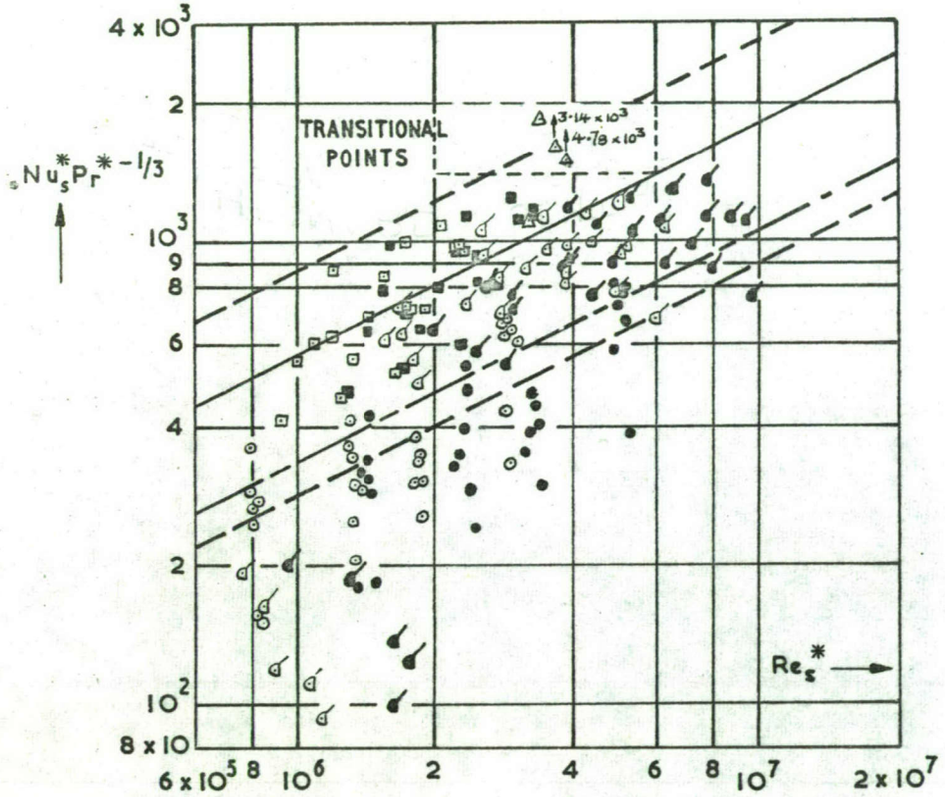

FIG. 9

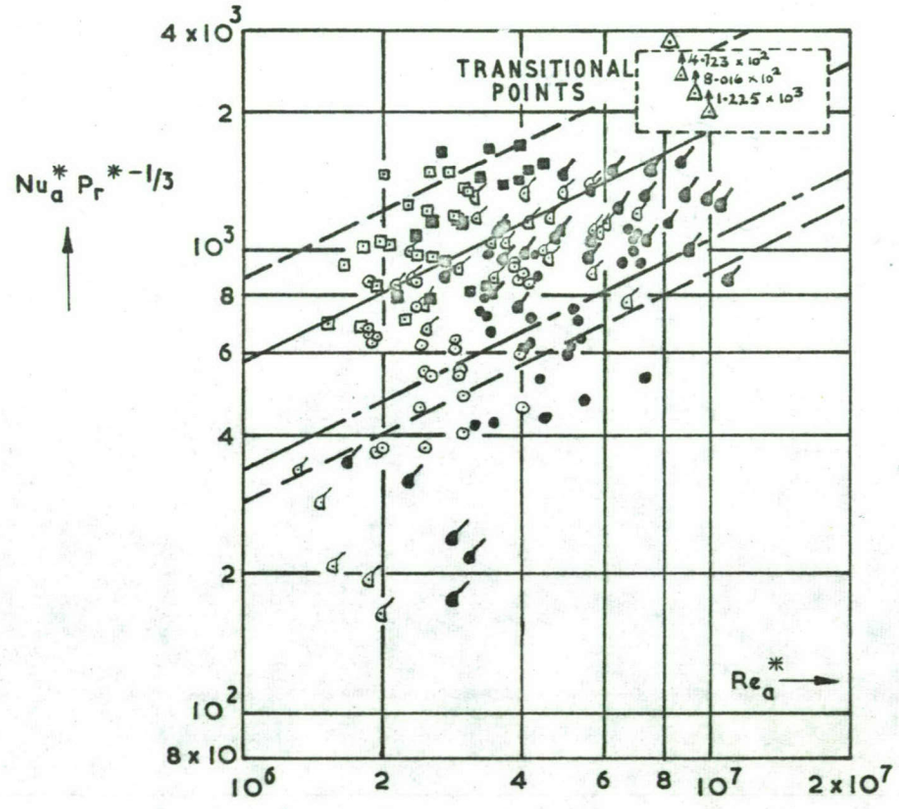

FIG. 10

——— CONE THEORY, $\sqrt{3}$ x FLAT PLATE THEORY.

——— · ——— FLAT PLATE THEORY, $Nu^* Pr^{*-1/3} = 0.332\ Re^{*1/2}$

– – – – – – CONE THEORY + OR − 50%

FIGS. 9 & 10. VARIATION OF $Nu_s^* Pr^{*-1/3}$ AND $Nu_a^* Pr^{*-1/3}$ WITH Re_s^* AND Re_a^* RESPECTIVELY FOR FREE FLIGHT TESTS ON CONICAL SKIRTS. LAMINAR FLOW.

CONFIDENTIAL

FIGS. 9 & 10

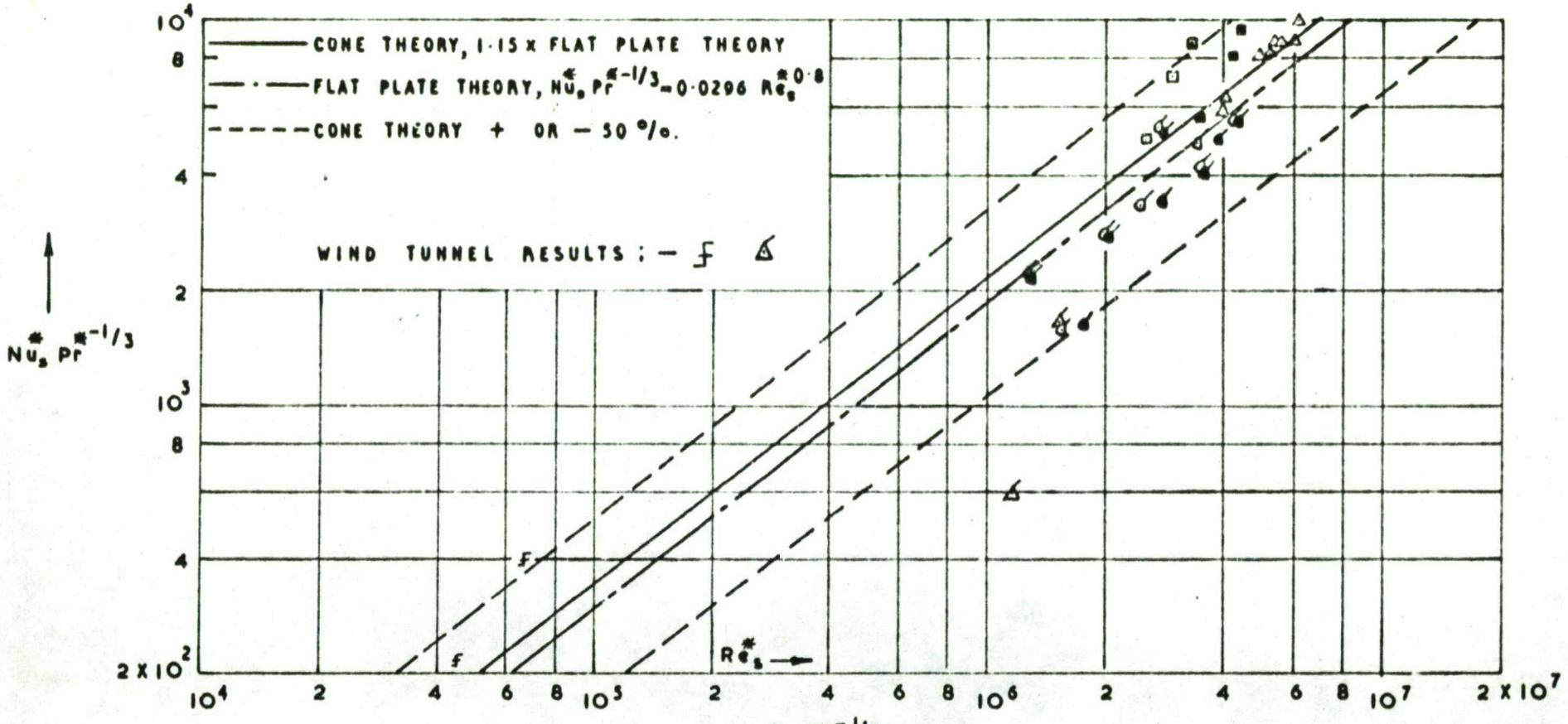

FIG. 11. $Nu_s^* Pr^{*-1/3}$ VS Re_s^*

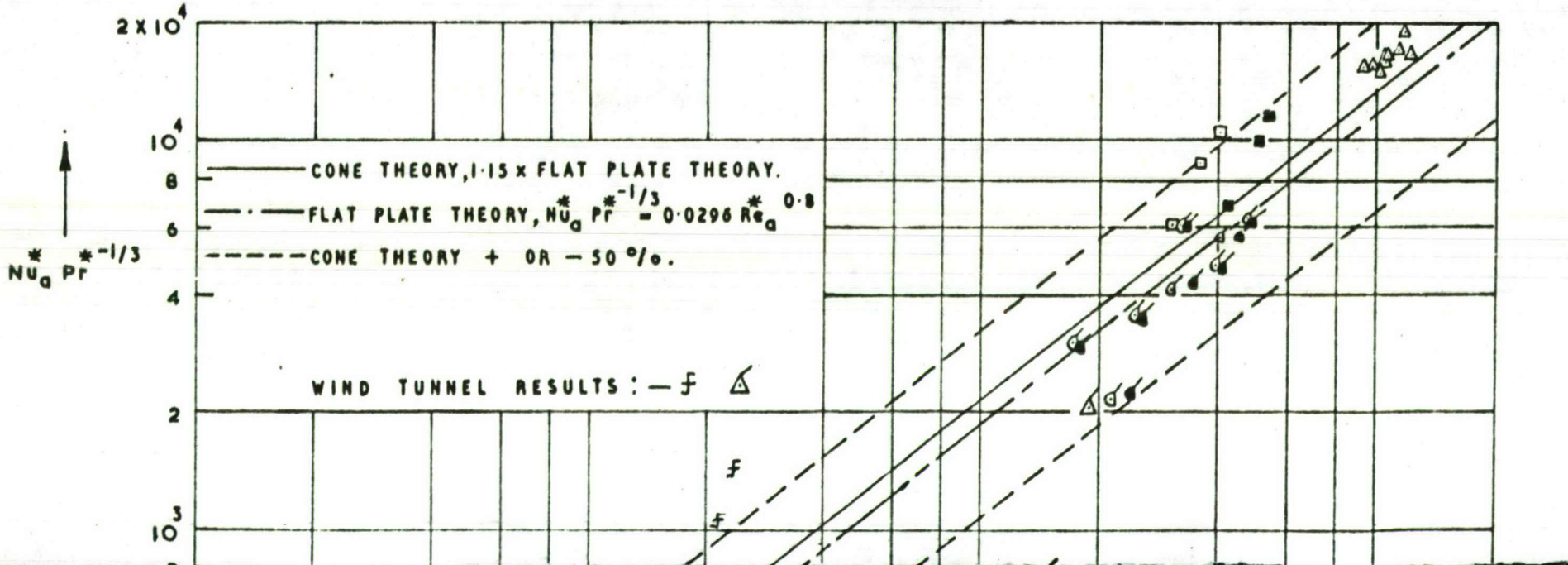

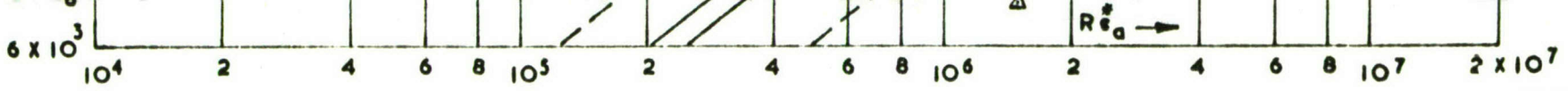

FIG. 12. $N\overset{*}{u}_a \, Pr^{*-1/3}$ VS $R\overset{*}{e}_a$

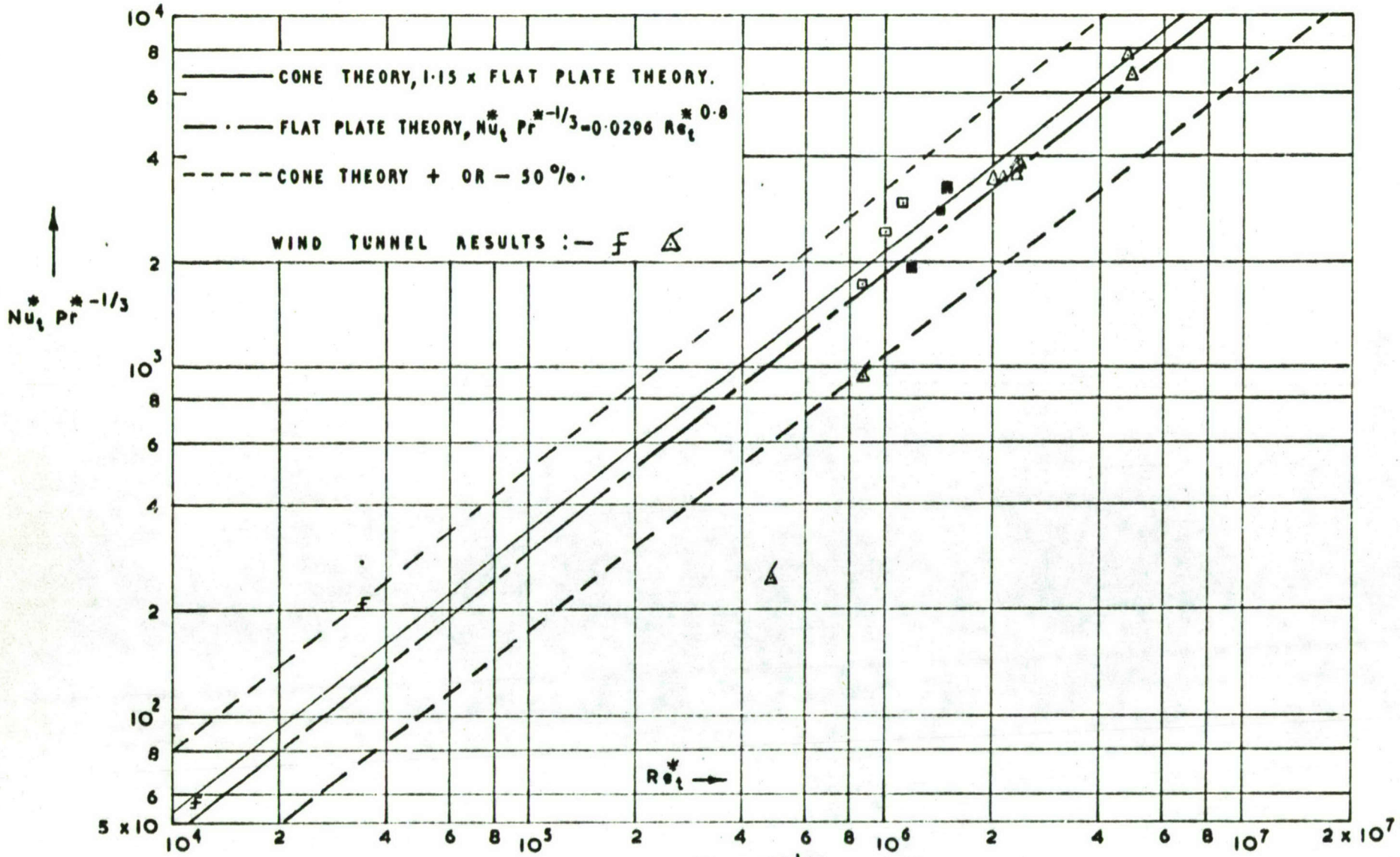

FIG. 13. $N\overset{*}{u}_t \, P_r^{*-1/3}$ VS. $R\overset{*}{e}_t$

NORMAL SHOCK WAVE CONDITIONS:- ◁ □ f Δ ; CONICAL SHOCK WAVE CONDITIONS:- ◀ ■

FIGS. 11. 12 & 13. VARIATION OF $N\overset{*}{u}_s \, Pr^{*-1/3}$, $N\overset{*}{u}_a \, Pr^{*-1/3}$ AND $N\overset{*}{u}_t \, Pr^{*-1/3}$ WITH $R\overset{*}{e}_s$, Re_a AND $R\overset{*}{e}_t$ RESPECTIVELY, FOR WIND TUNNEL AND FREE FLIGHT TESTS ON CONICAL SKIRTS. TURBULENT FLOW.

CONFIDENTIAL

FIGS. 11. 12 & 13.

(12)

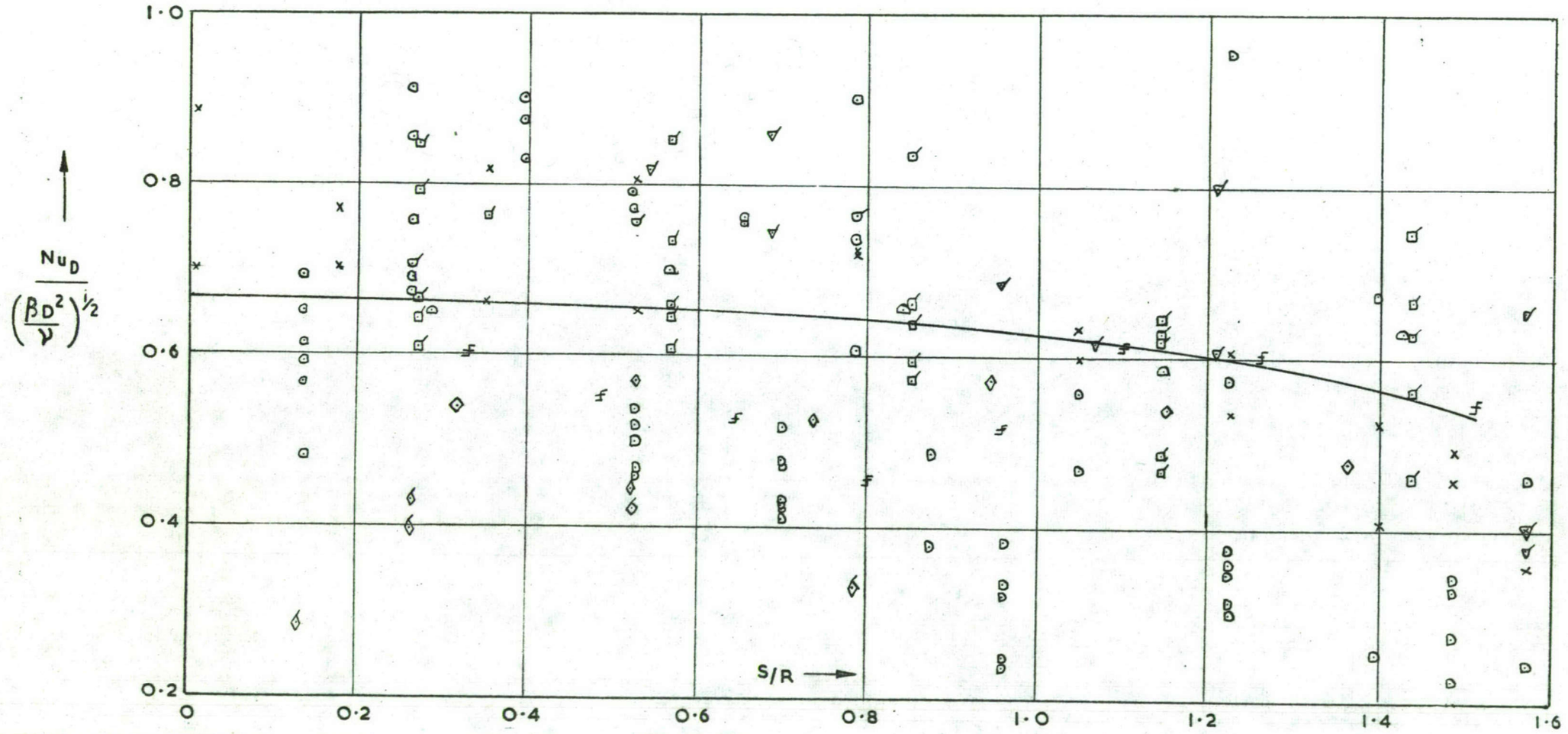

FIG. 14. VARIATION OF THE HEAT TRANSFER PARAMETER, $Nu_D/(\beta D^2/\nu)^{1/2}$, WITH S/R FOR WIND TUNNEL TESTS ON HEMISPHERES AND BLUNT CONE NOSE CAPS. LAMINAR FLOW.

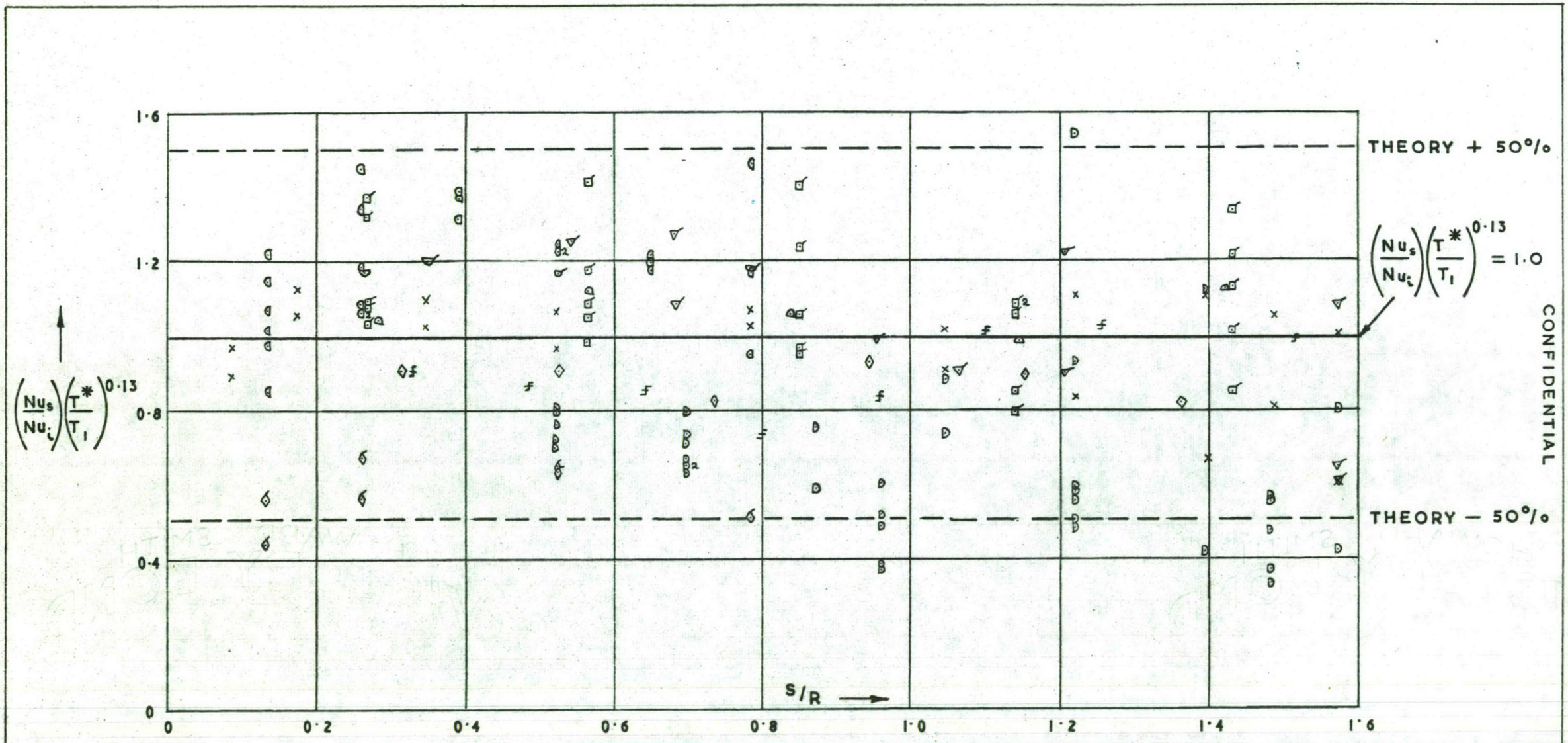

FIG. 15 VARIATION OF THE PARAMETER $\left(Nu_s/Nu_i\right)\left(T^*/T_1\right)^{0.13}$ WITH S/R FOR WIND TUNNEL TESTS ON HEMISPHERES AND BLUNT CONE NOSE CAPS. LAMINAR FLOW.

CONFIDENTIAL

FIG. 15

CONFIDENTIAL

FIG. 15

VARIATION OF THE PARAMETER $\frac{M_{ns}}{M_{ns^2}}\left(\frac{T_1}{T^*}\right)^{0.12}$ WITH s/R FOR WIND TUNNEL TESTS ON HEMISPHERES AND BLUNT CONE AFTERBODIES WITH SUPERSONIC LAMINAR BASE FLOW

THEORY − 20%

THEORY + 20%

$\frac{M_{ns}}{M_{ns^2}}\left(\frac{T_1}{T^*}\right)^{0.12} = 1.0$

s/R

0.2 0.4 0.6 0.8 1.0 1.2 1.4 1.6

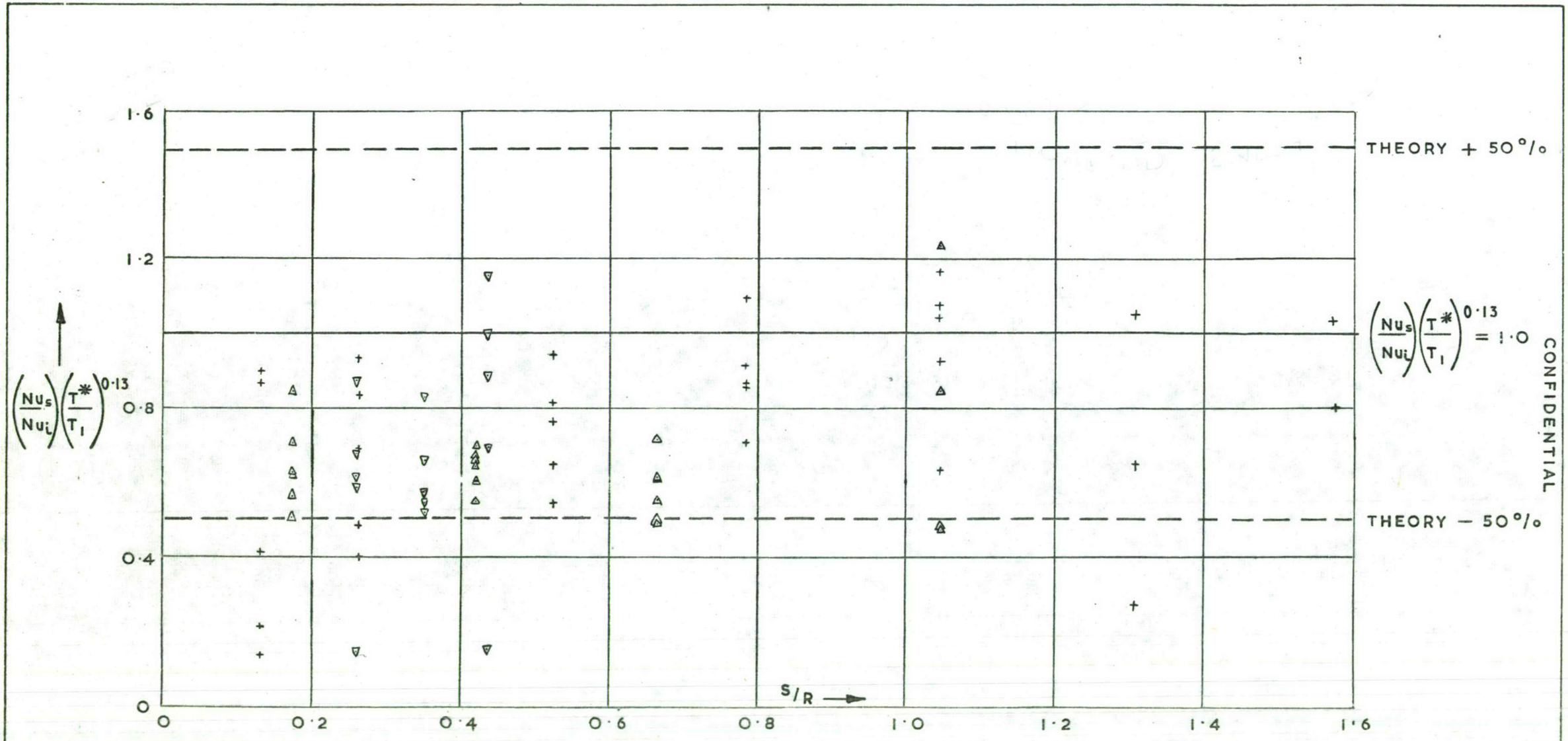

FIG. 16 VARIATION OF THE PARAMETER $\left(Nu_s/Nu_i\right)\left(T^*/T_1\right)^{0\cdot13}$ WITH S/R FOR FREE FLIGHT TESTS ON HEMISPHERES AND BLUNT CONE NOSE CAPS. LAMINAR FLOW.

CONFIDENTIAL

FIG. 16.

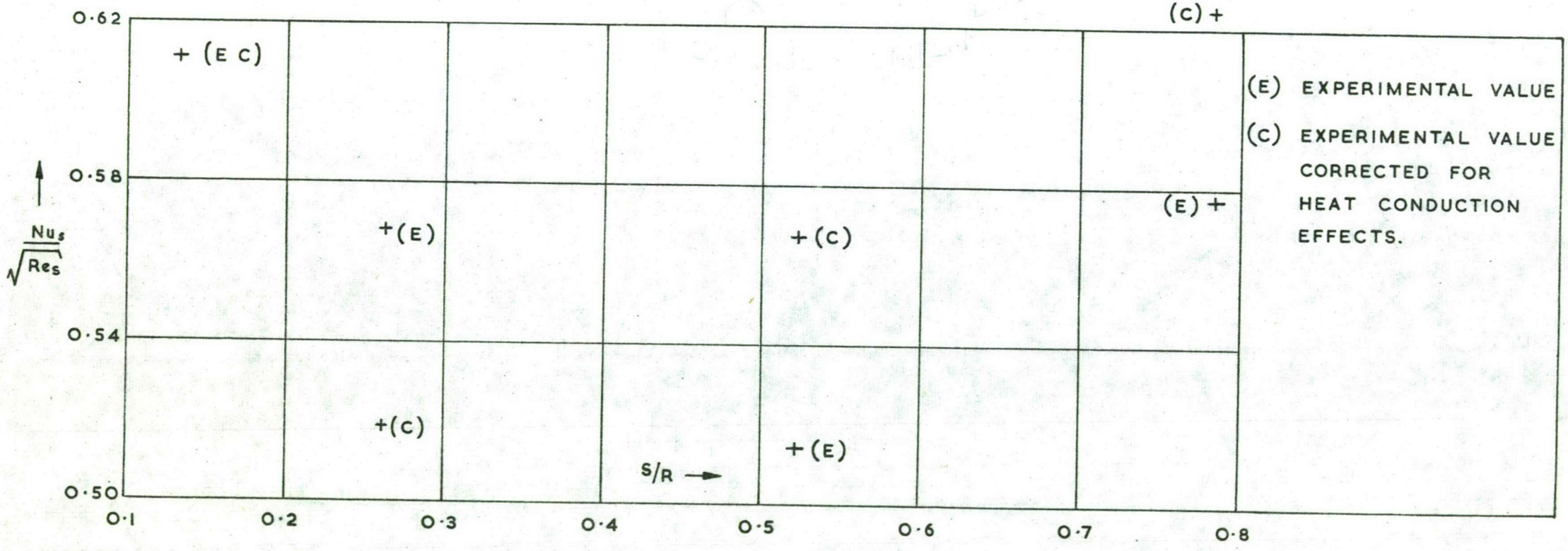

FIG. 17. EFFECT OF LONGITUDINAL HEAT CONDUCTION ON THE LAMINAR HEAT TRANSFER PARAMETER, $Nu_s/\sqrt{Re_s}$, FOR THE HEMISPHERE TESTED IN REF. 6 AT A FLIGHT TIME OF 5·0 SECONDS.

CONFIDENTIAL

FIG. 17.

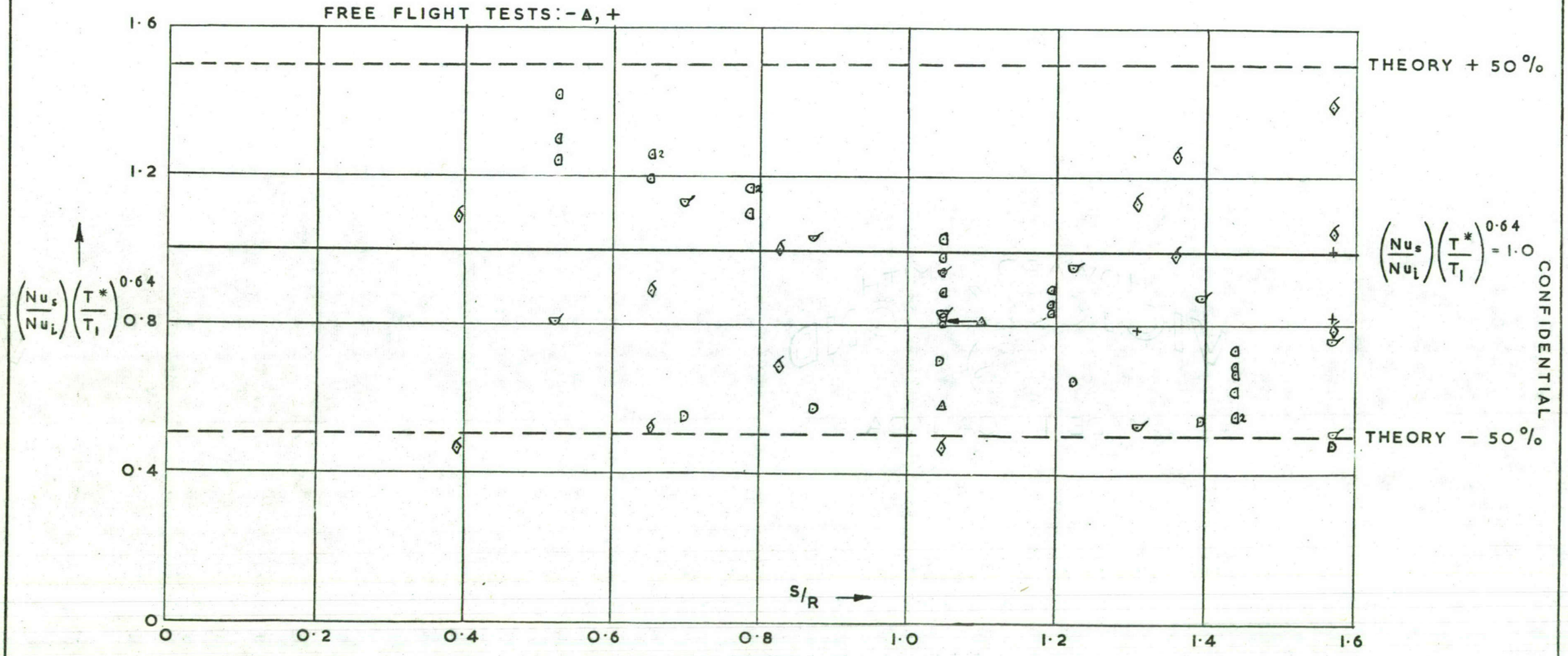

FIG. 18 VARIATION OF THE PARAMETER $(Nu_s/Nu_i)(T^*/T_1)^{0.64}$ WITH S/R FOR FREE FLIGHT AND WIND TUNNEL TESTS ON HEMISPHERES AND BLUNT CONE NOSE CAPS. TURBULENT FLOW.

FIG. 18.

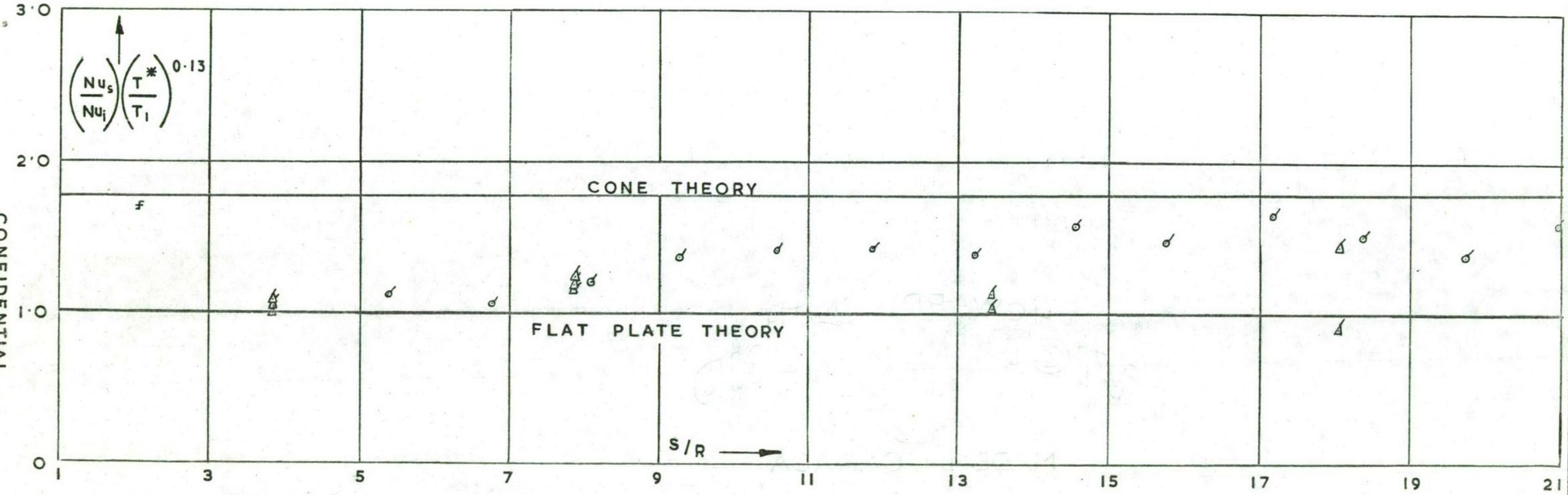

FIG. 19. VARIATION OF THE PARAMETER $(Nu_s/Nu_i)(T^*/T_1)^{0.13}$ WITH S/R FOR WIND TUNNEL TESTS ON CONE SKIRTS. LAMINAR FLOW.

FIG. 19.

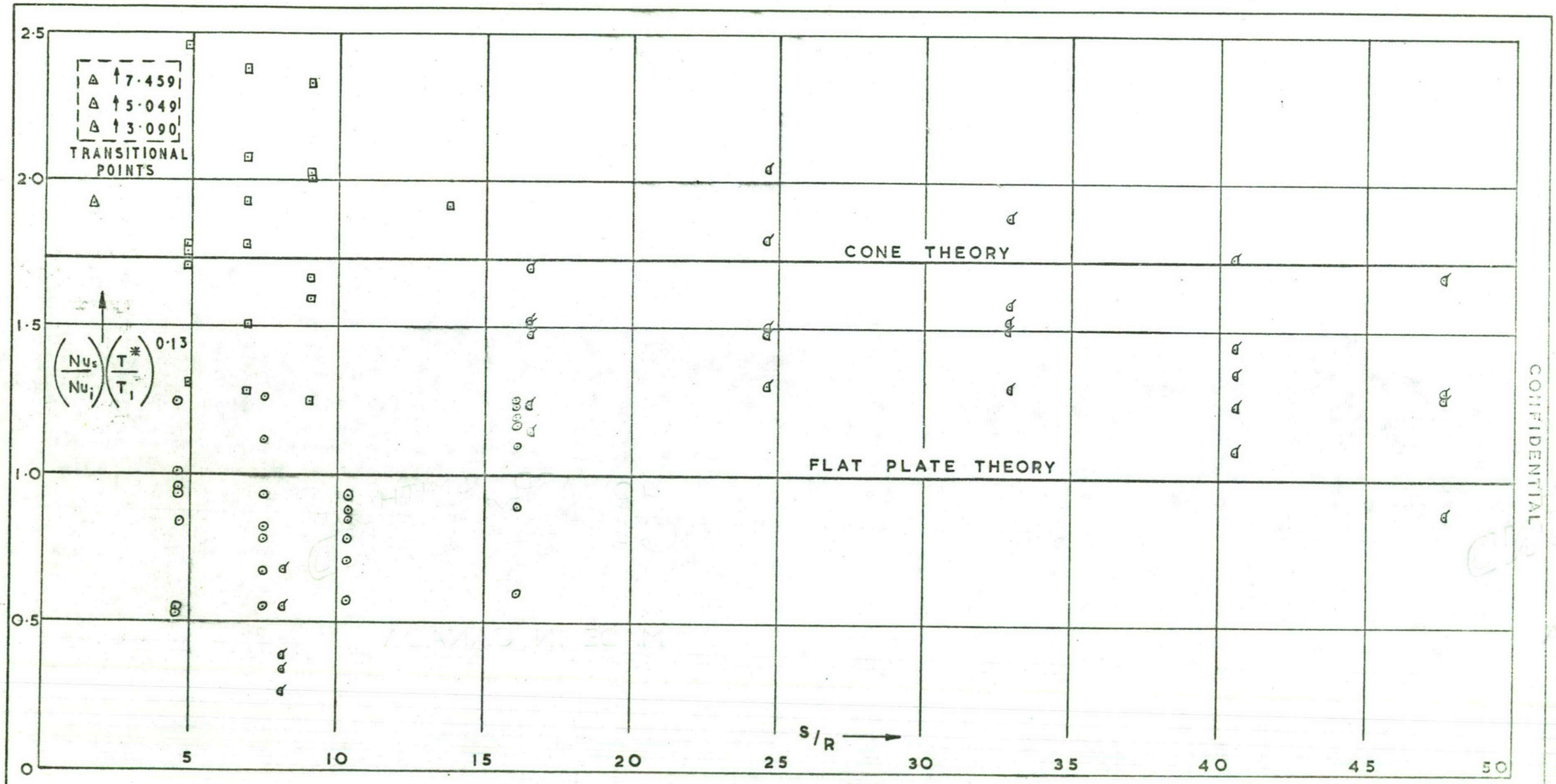

FIG. 20. VARIATION OF THE PARAMETER $\left(Nu_s/ Nu_i\right)\left(T^*/ T_1\right)^{0.13}$ WITH S/R FOR FREE FLIGHT TESTS ON CONICAL SKIRTS. LAMINAR FLOW, WITH ALL POINTS BASED ON A NORMAL SHOCK WAVE.

FIG. 20.

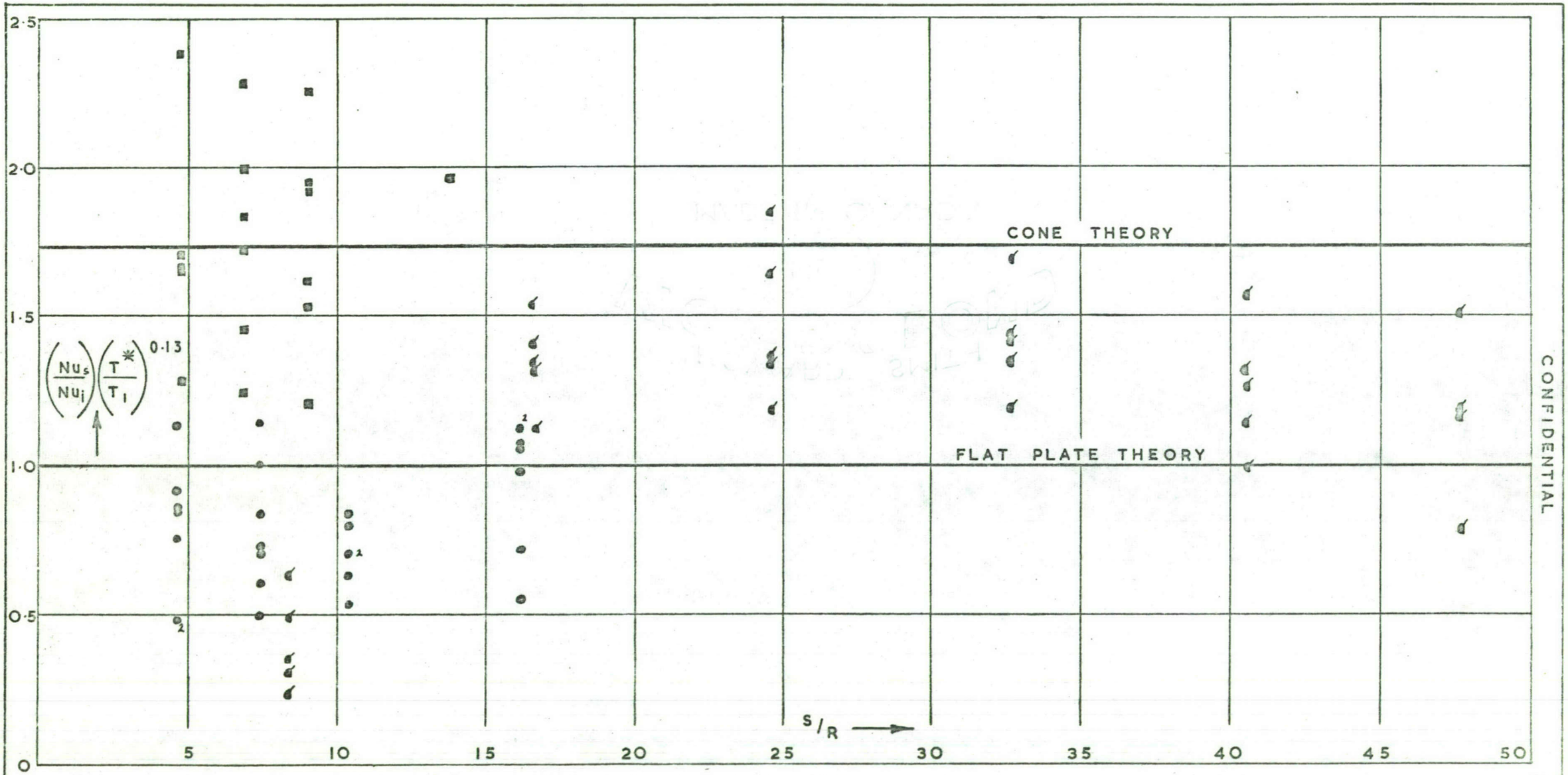

CONFIDENTIAL

FIG. 21. VARIATION OF THE PARAMETER $\left(Nu_s/Nu_i\right)\left(T^*/T_1\right)^{0.13}$ WITH S/R FOR FREE FLIGHT TESTS ON CONICAL SKIRTS. LAMINAR FLOW, WITH ALL POINTS BASED ON A CONICAL SHOCK WAVE.

FIG. 21.

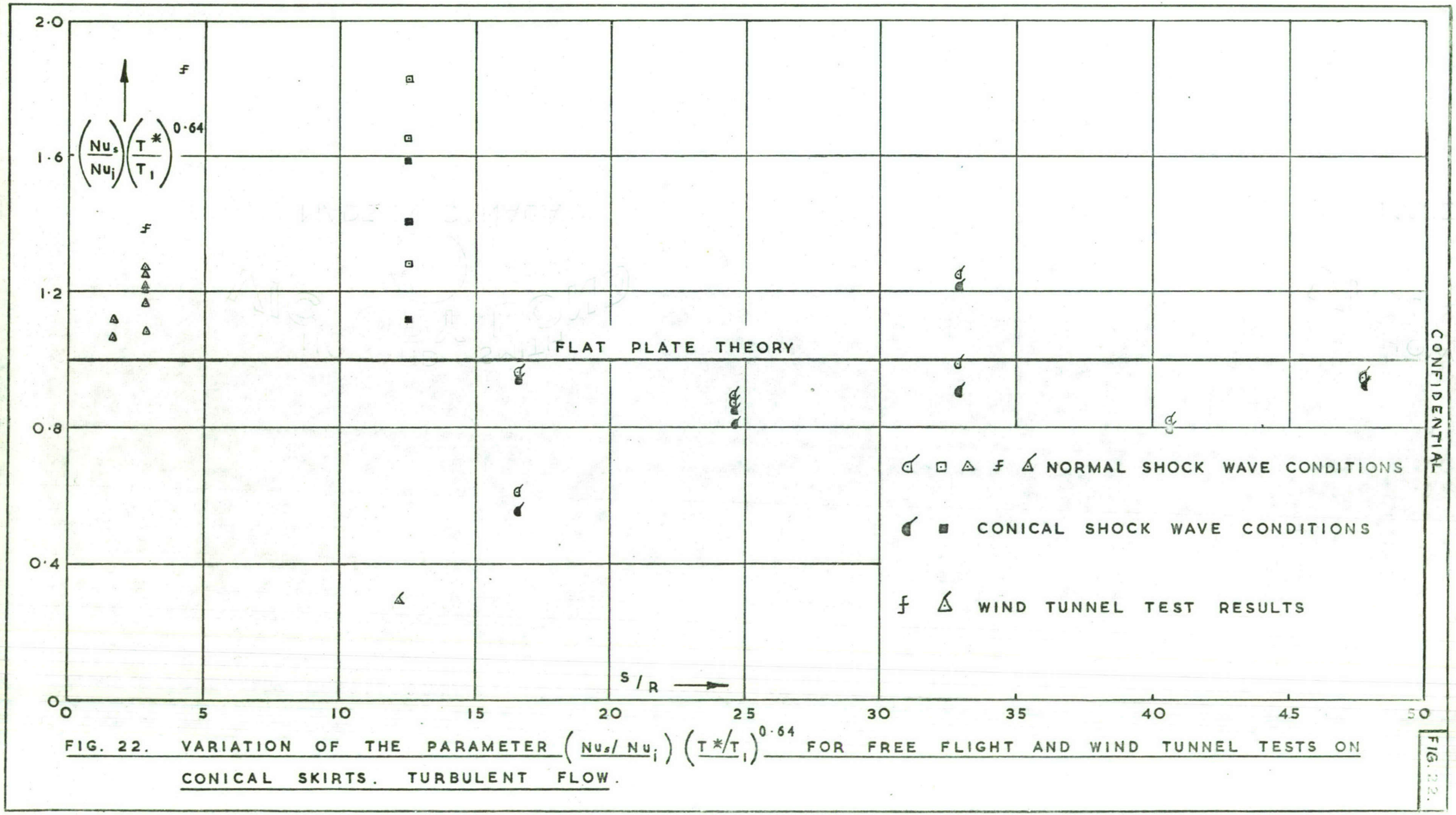

FIG. 22. VARIATION OF THE PARAMETER $\left(Nu_s/Nu_i\right)\left(T^*/T_1\right)^{0.64}$ FOR FREE FLIGHT AND WIND TUNNEL TESTS ON CONICAL SKIRTS. TURBULENT FLOW.

FIG. 22.

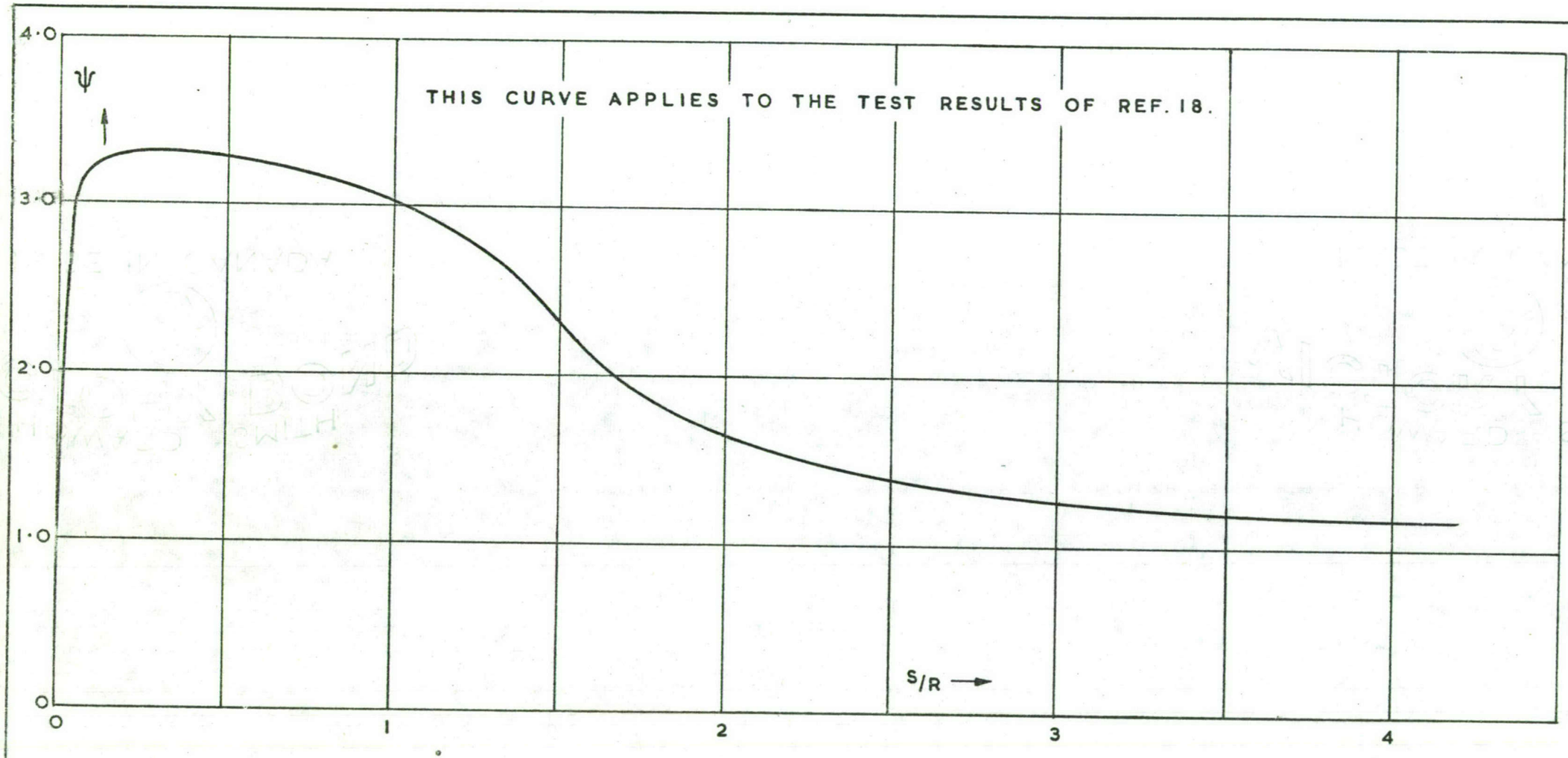

FIG. 23. THE PRESSURE GRADIENT PARAMETER ψ FOR LAMINAR FLOW OVER A HEMISPHERE CONE FOR $M\infty = 3 \cdot 12$ $T_w / T_o = 1 \cdot 0$ AND $\theta_c = 4 \cdot 75°$.

CONFIDENTIAL

FIG. 23.

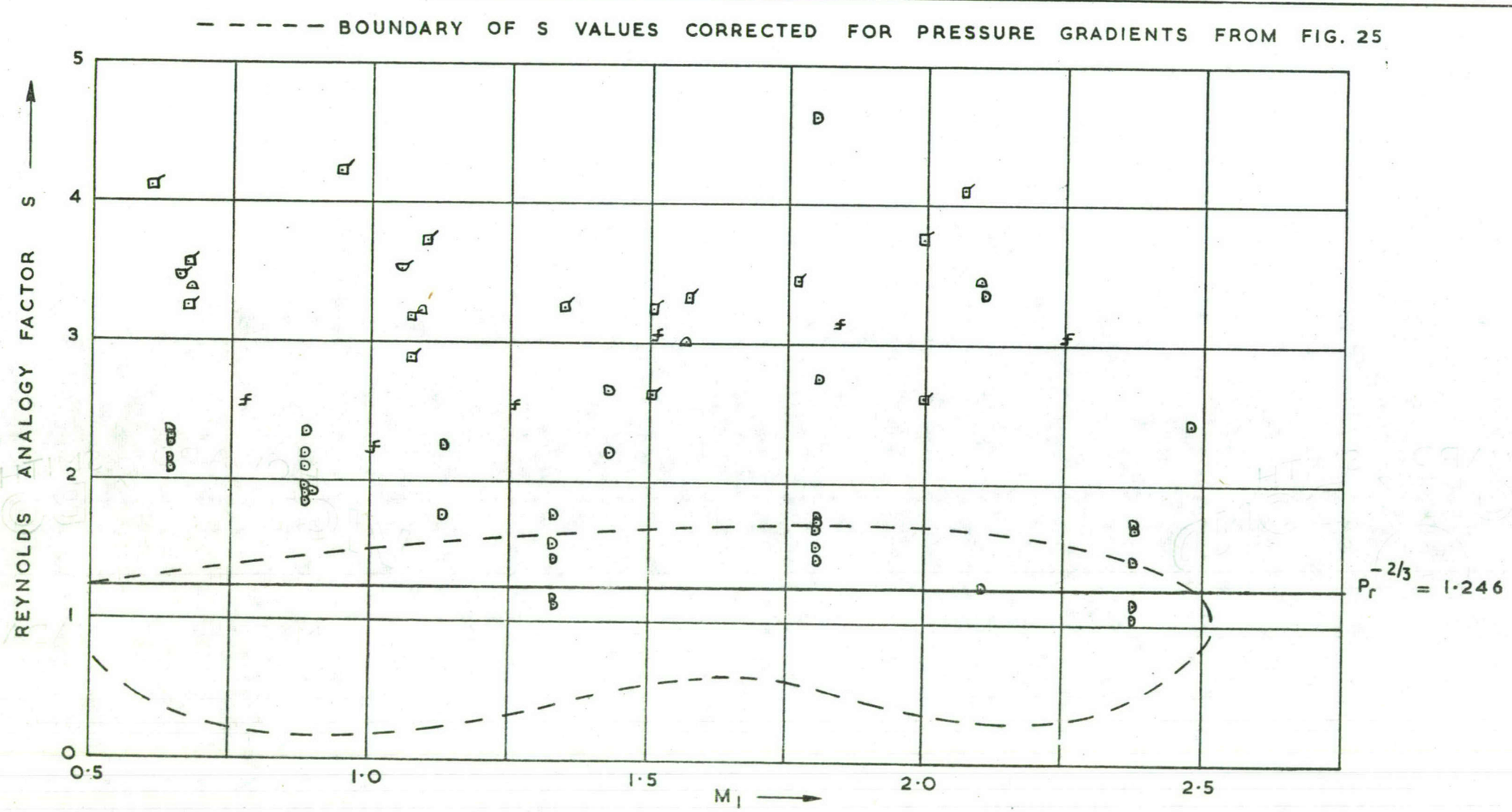

FIG. 24. VARIATION OF REYNOLDS ANALOGY FACTOR WITH LOCAL MACH NUMBER FOR WIND TUNNEL TESTS ON HEMISPHERES AND CONE CAPS. LAMINAR FLOW. (UNCORRECTED FOR PRESSURE GRADIENTS)

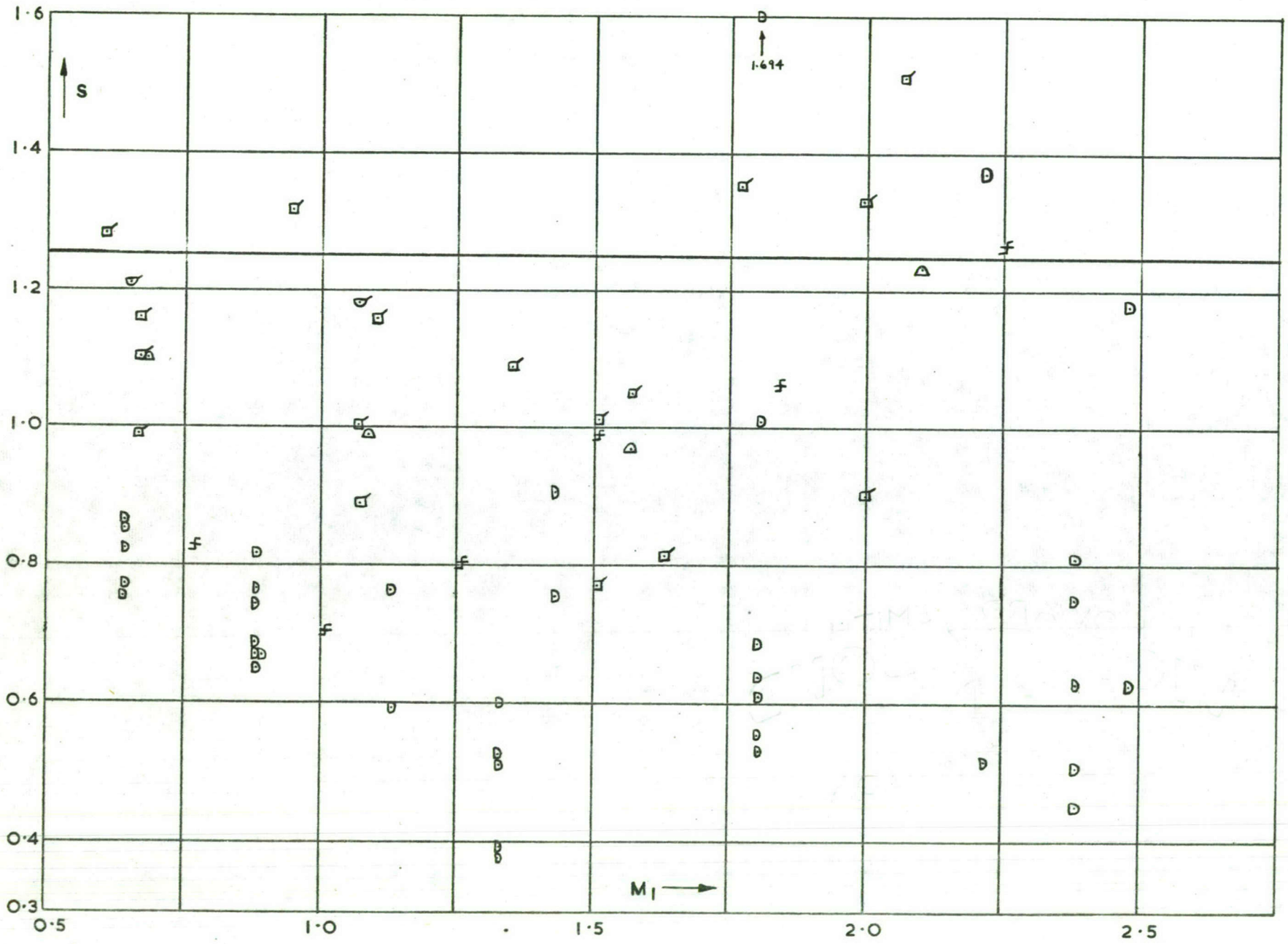

$P_r^{-2/3} = 1 \cdot 246$

RESULTS FOR WIND TUNNEL TESTS ON HEMISPHERES AND NOSE CAPS. LAMINAR FLOW.

CONFIDENTIAL

FIG. 25

FIG. 25. REYNOLDS ANALOGY FACTOR CORRECTED FOR PRESSURE GRADIENTS VS. LOCAL MACH NUMBER.

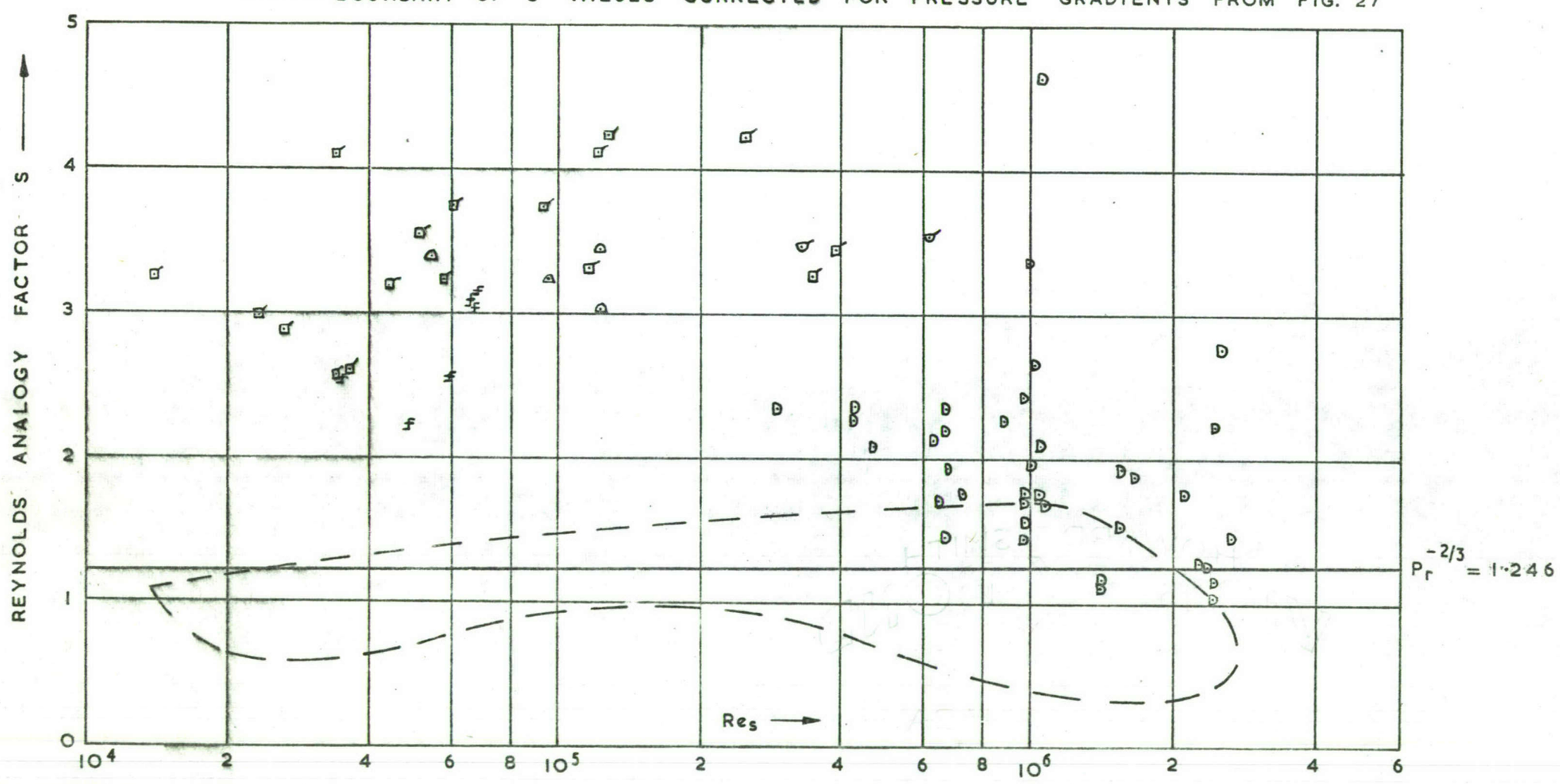

FIG. 26. VARIATION OF REYNOLDS ANALOGY FACTOR WITH LOCAL REYNOLDS NUMBER FOR WIND TUNNEL TESTS ON HEMISPHERES AND CONE CAPS. LAMINAR FLOW. (UNCORRECTED FOR PRESSURE GRADIENTS)

CONFIDENTIAL

FIG. 26.

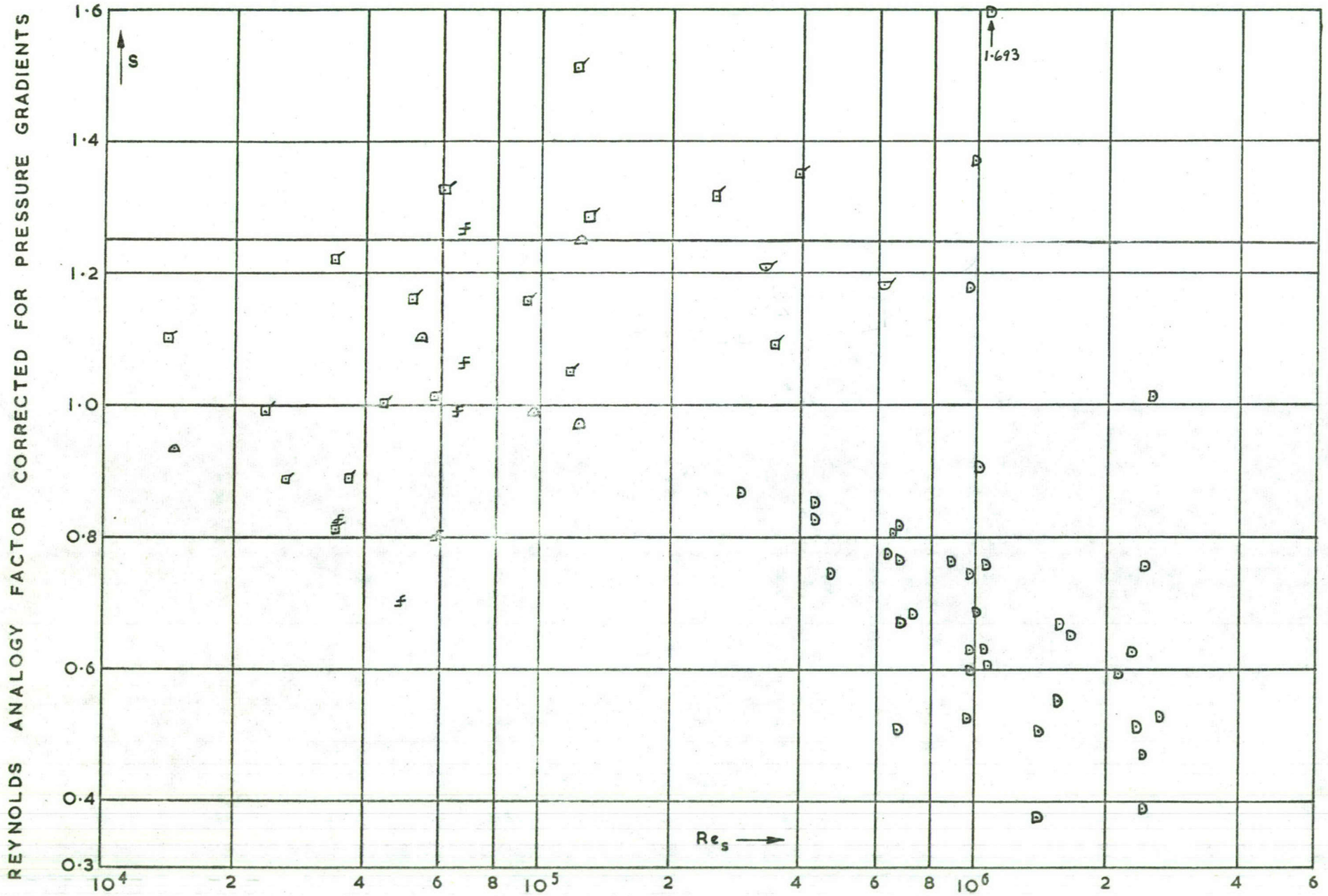

FIG. 27. REYNOLDS ANALOGY FACTOR CORRECTED FOR PRESSURE GRADIENTS VS. LOCAL REYNOLDS NUMBER

CONFIDENTIAL

FIG. 27

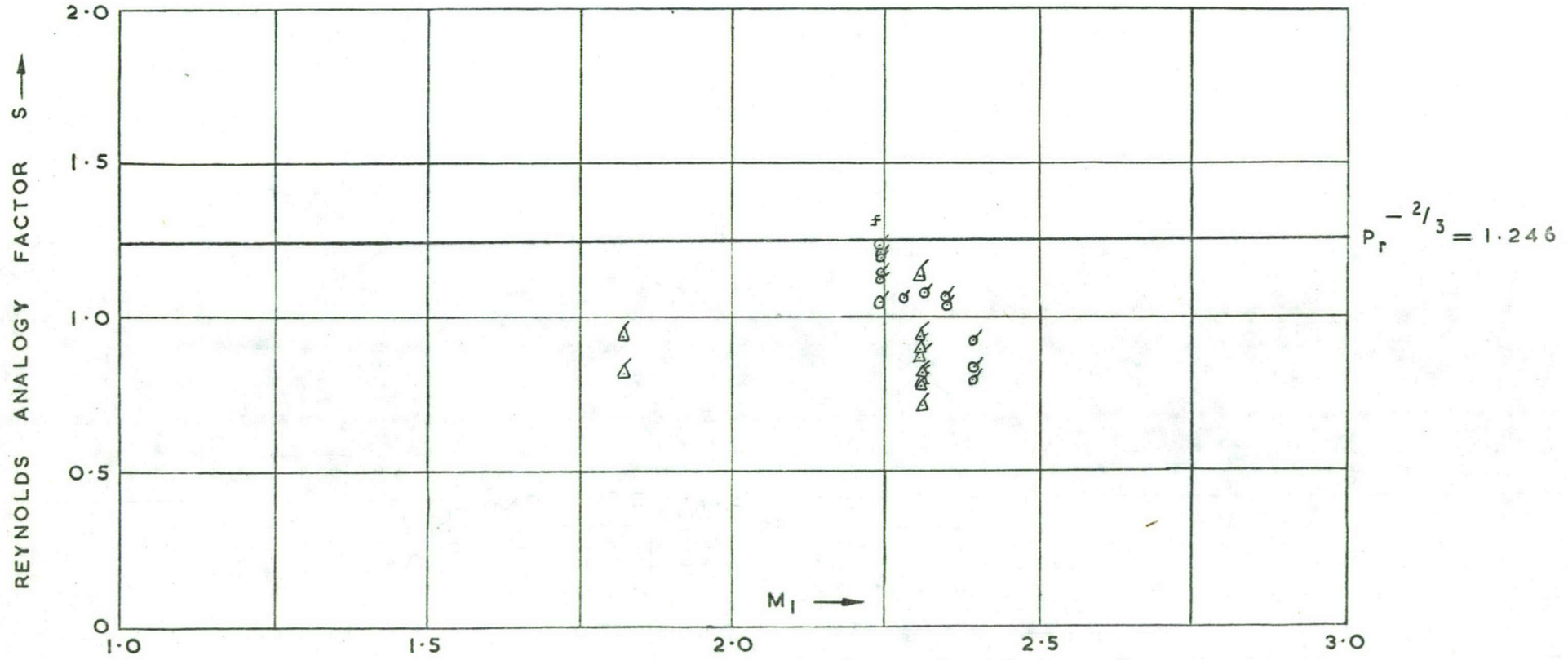

FIG. 28. VARIATION OF REYNOLDS ANALOGY FACTOR WITH LOCAL MACH NUMBER FOR WIND TUNNEL TESTS ON CONE SKIRTS. LAMINAR FLOW.

FIG. 29

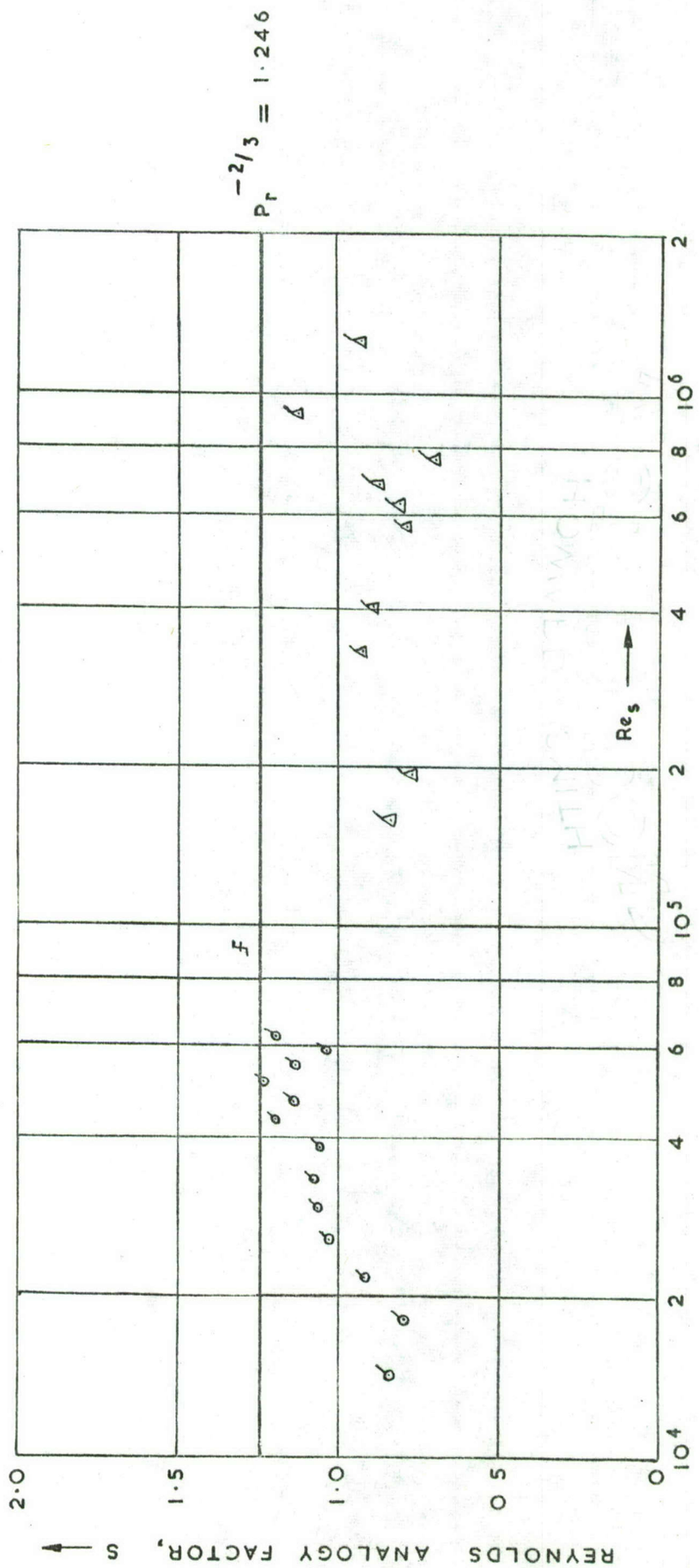

FIG. 29. VARIATION OF REYNOLDS ANALOGY FACTOR WITH LOCAL REYNOLDS NUMBER FOR WIND TUNNEL TESTS ON CONE SKIRTS. LAMINAR FLOW.

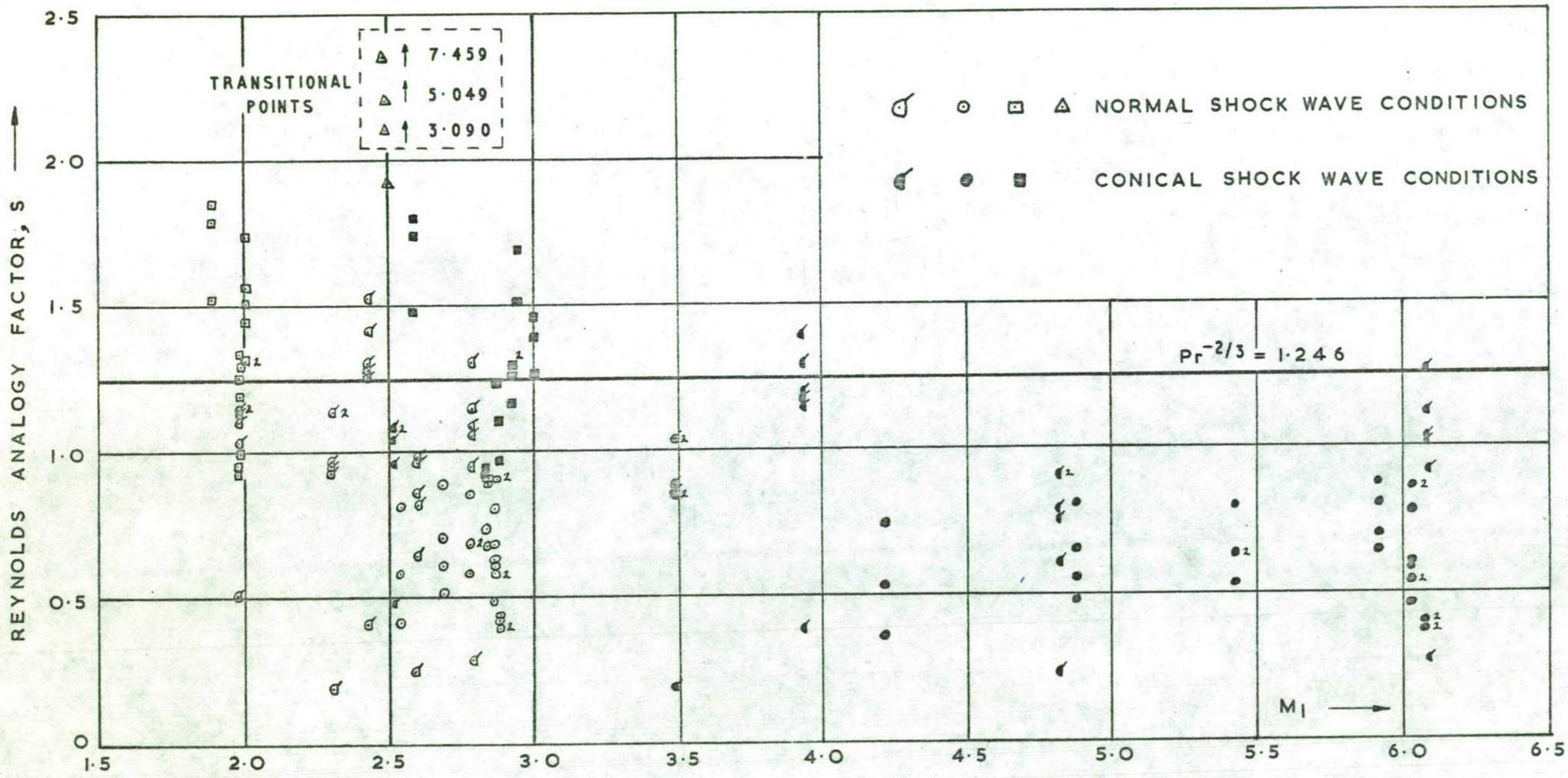

FIG. 30. VARIATION OF REYNOLDS ANALOGY FACTOR WITH LOCAL MACH NUMBER FOR FREE FLIGHT TESTS ON CONICAL SKIRTS. LAMINAR FLOW.

CONFIDENTIAL

FIG. 30.

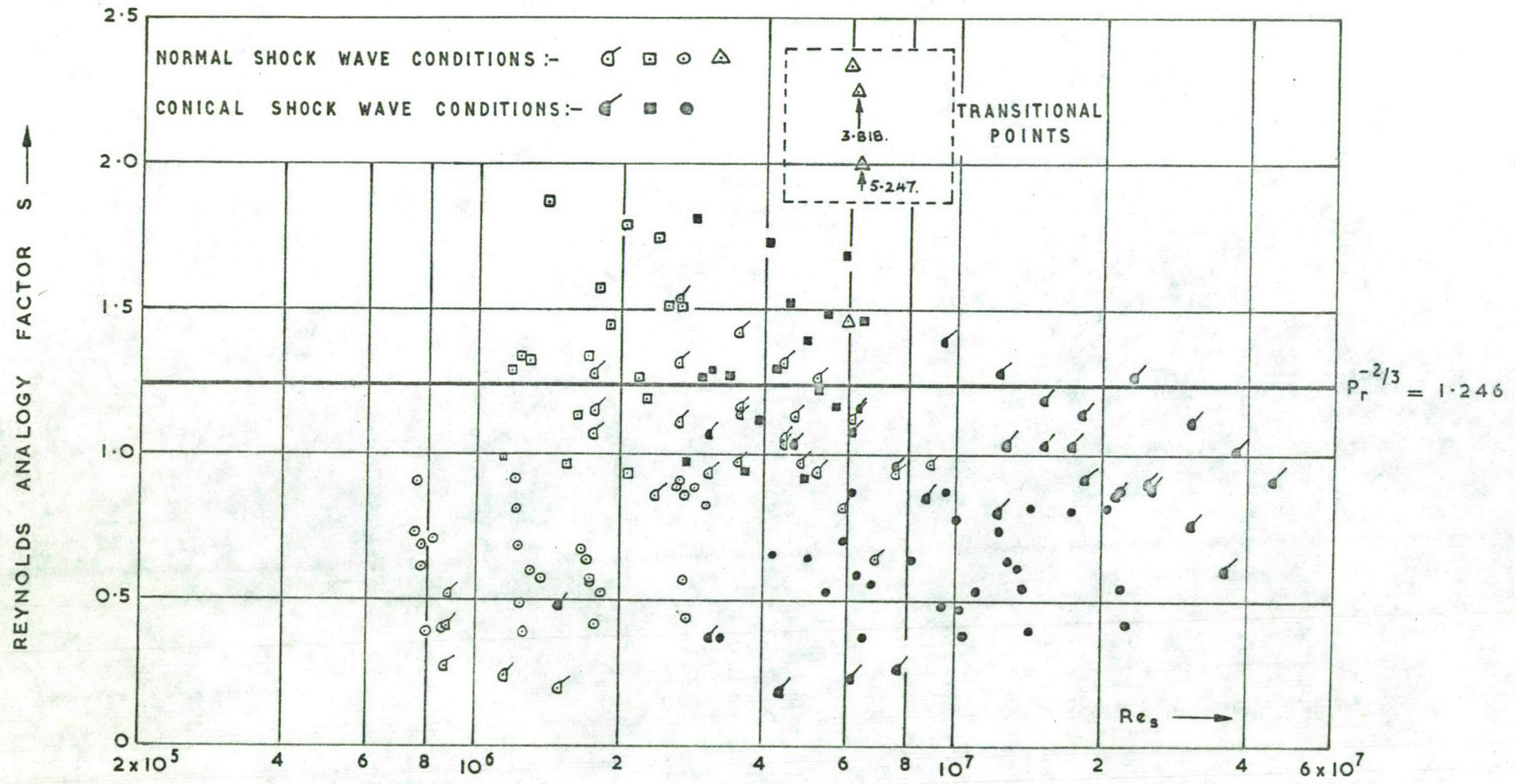

FIG. 31. VARIATION OF REYNOLDS ANALOGY FACTOR WITH LOCAL REYNOLDS NUMBER FOR FREE FLIGHT TESTS ON CONICAL SKIRTS. LAMINAR FLOW.

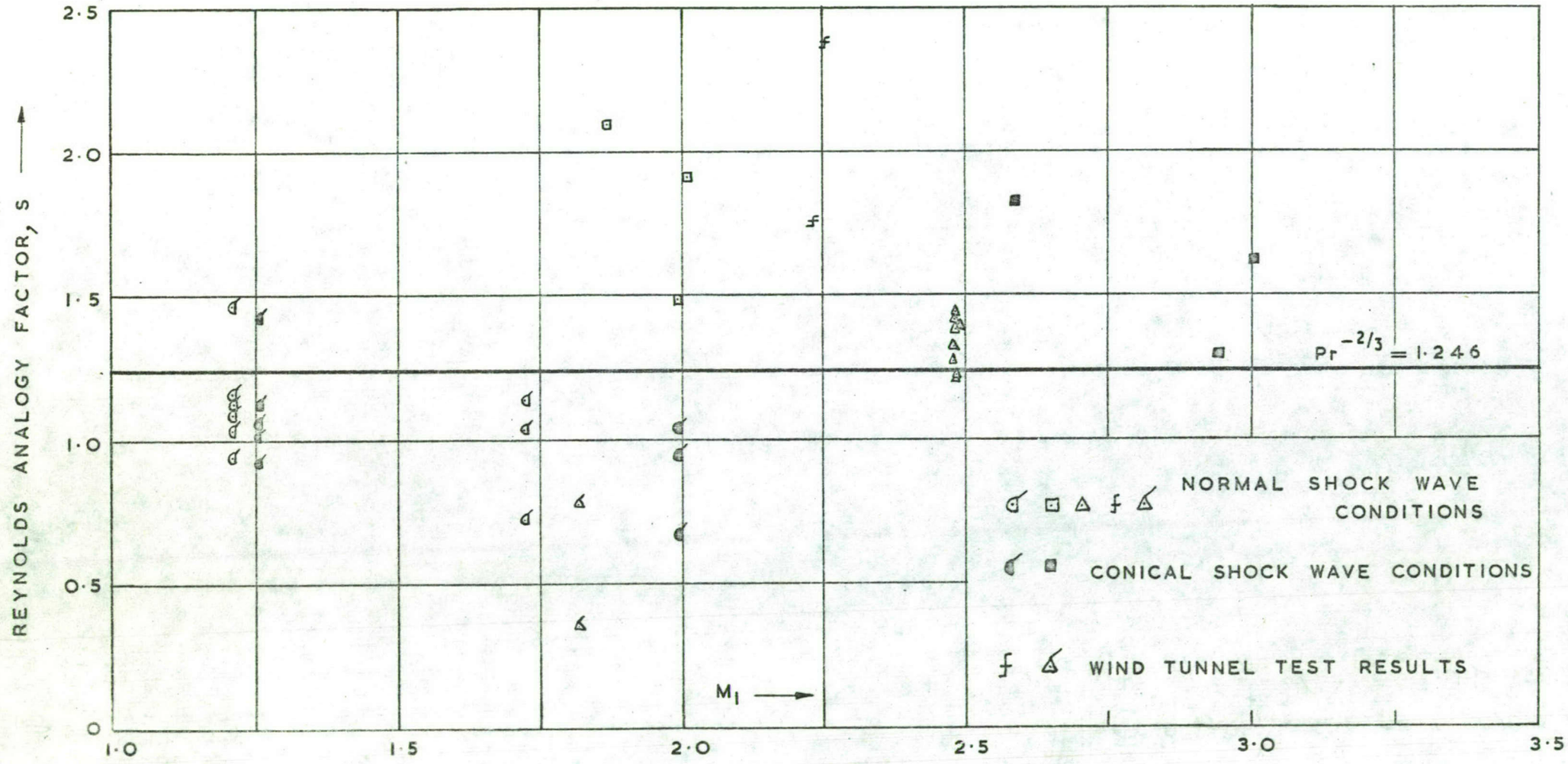

FIG. 32. VARIATION OF REYNOLDS ANALOGY FACTOR WITH LOCAL MACH NUMBER FOR FREE FLIGHT AND WIND TUNNEL TESTS ON CONICAL SKIRTS. TURBULENT FLOW.

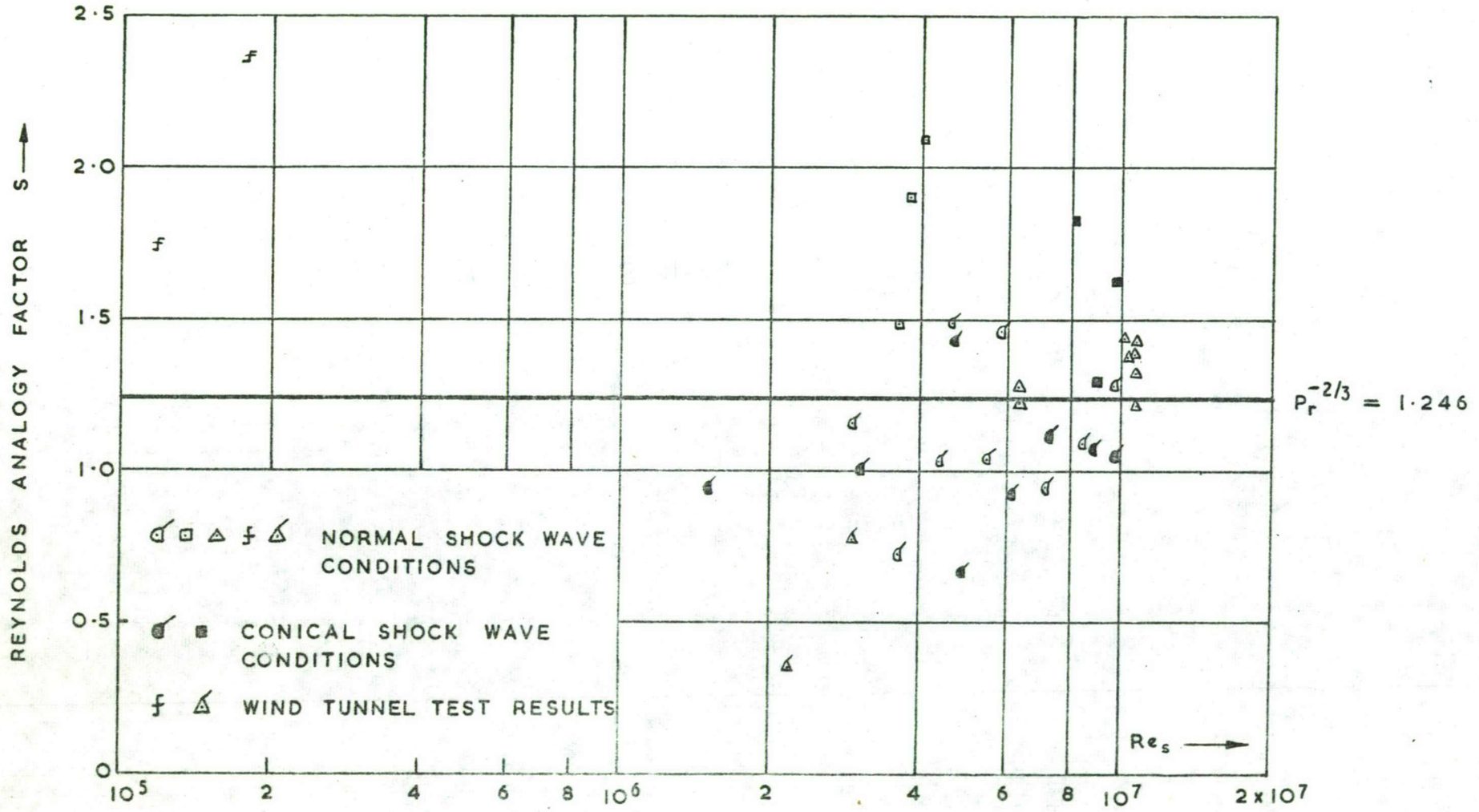

FIG. 33 VARIATION OF REYNOLDS ANALOGY FACTOR, WITH LOCAL REYNOLDS NUMBER, FOR FREE FLIGHT AND WIND TUNNEL TESTS ON CONICAL SKIRTS. TURBULENT FLOW.

CONFIDENTIAL

FIG. 33

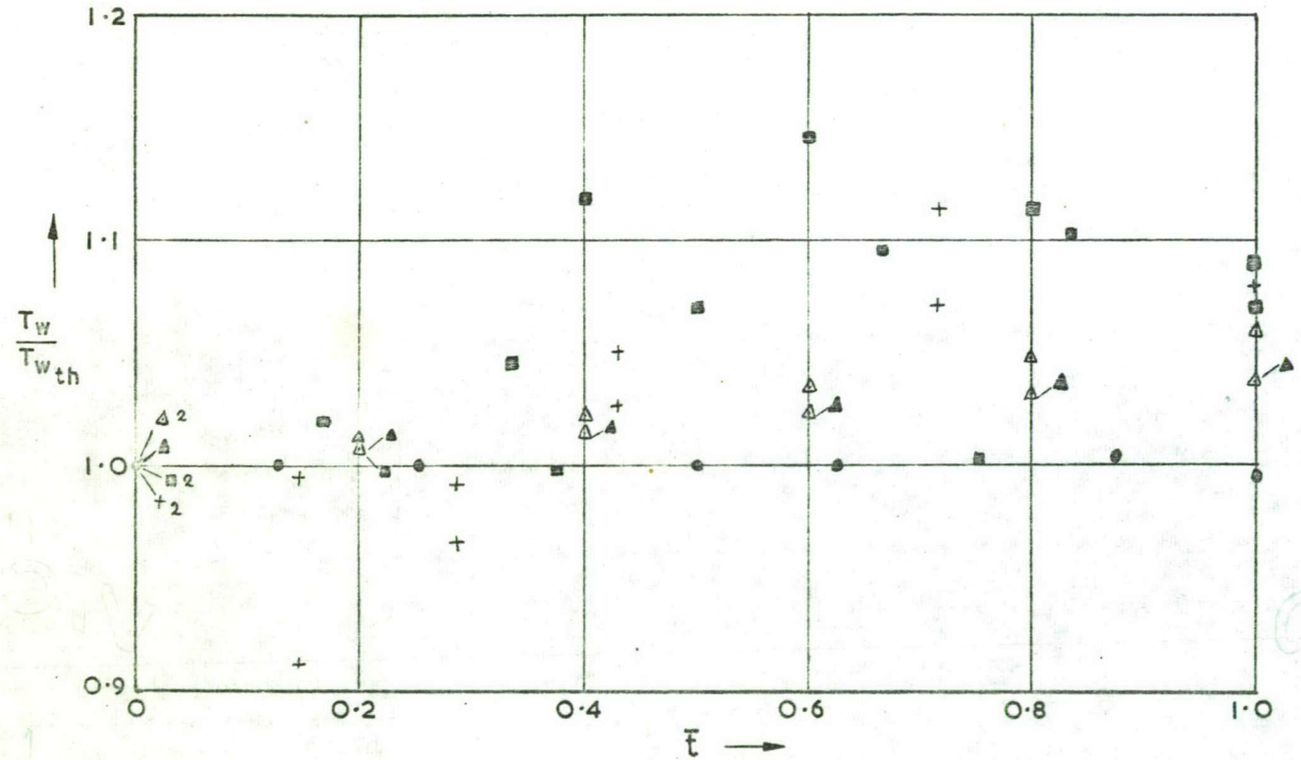

NOTE:-

+ & OPEN SYMBOLS REPRESENT STATIONS ON NOSE CAPS

BLACK SYMBOLS REPRESENT STATIONS ON CONE SKIRTS

REDUCED FLIGHT TIME $\bar{t}$ IS DEFINED AS

$$\bar{t} = \frac{t - t_{min}}{t_{max} - t_{min}}$$

& t = CURRENT TIME

t_{min} = TIME FOR FIRST DATA POINT

t_{max} = TIME AT WHICH MEASURED T_w IS A MAXIMUM.

FIG. 34. RATIO OF MEASURED WALL TEMPERATURES TO THEORETICAL WALL TEMPERATURES VS REDUCED FLIGHT TIME, $\bar{t}$ FOR FOUR FREE FLIGHT TESTS.

CONFIDENTIAL

FIG. 34

Information Centre
Knowledge Services
[dstl] Porton Down
Salisbury
Wilts
SP4 0JQ
22060-6218
Tel: 01980-613753
Fax 01980-613970

Defense Technical Information Center (DTIC)
8725 John J. Kingman Road, Suit 0944
Fort Belvoir, VA 22060-6218
U.S.A.

AD#: AD333301

Date of Search: 28 July 2008

Record Summary: DSIR 23/29790
Title: A Correlation of Forced Convection Heat Transfer Measurements on Blunted Cones and Hemispheres for Mach Numbers up to 10.2 and Reynolds Numbers up to 4.5 x10 to the 7th Power
Availability Open Document, Open Description, Normal Closure before FOI Act: 30 years
Former reference (Department) ARC 23953
Held by The National Archives, Kew

This document is now available at the National Archives, Kew, Surrey, United Kingdom.

DTIC has checked the National Archives Catalogue website (http://www.nationalarchives.gov.uk) and found the document is available and releasable to the public.

Access to UK public records is governed by statute, namely the Public Records Act, 1958, and the Public Records Act, 1967.
The document has been released under the 30 year rule.
(The vast majority of records selected for permanent preservation are made available to the public when they are 30 years old. This is commonly referred to as the 30 year rule and was established by the Public Records Act of 1967).

This document may be treated as UNLIMITED.